A very-high-enery view of galactic nuclei

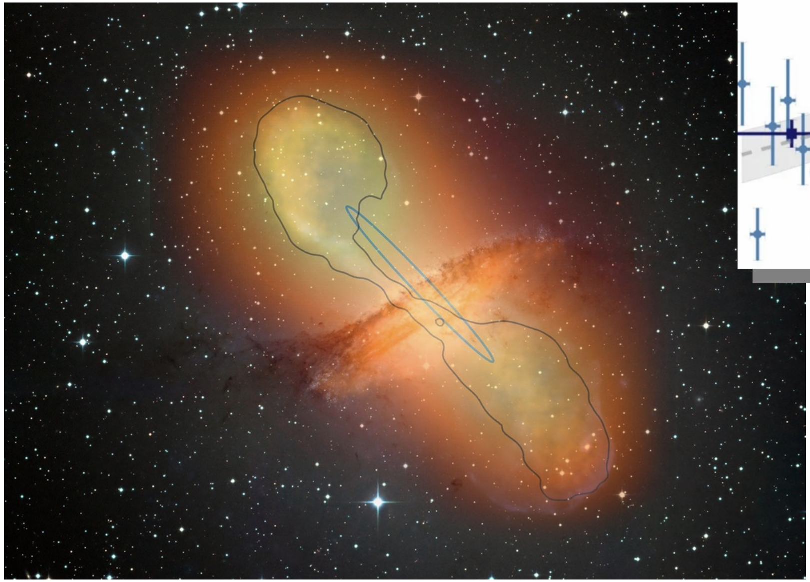

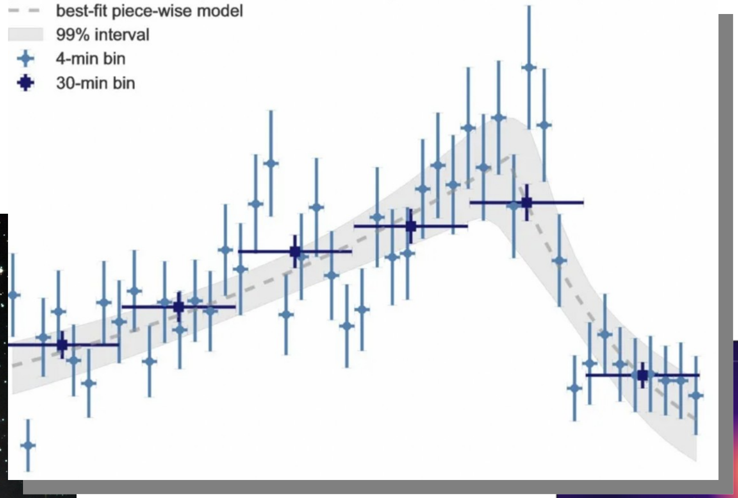

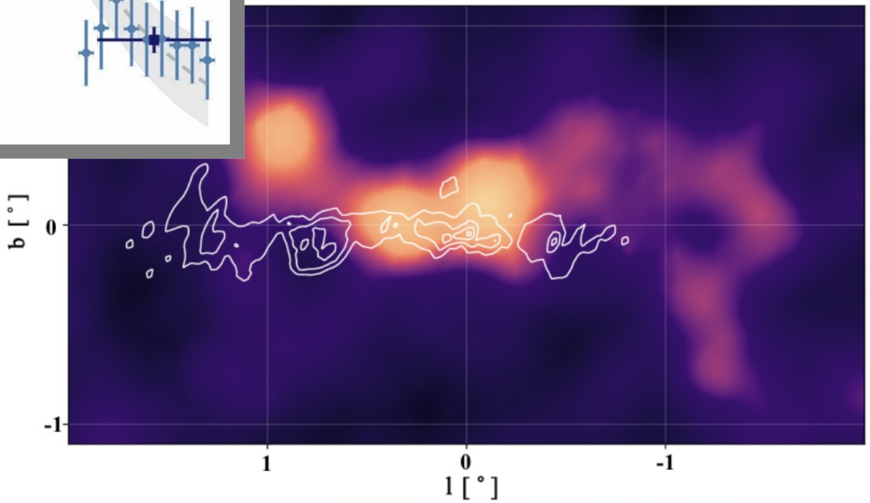

A. Zech

Gravity+ workshop 2024

LUTH Observatoire de Paris | PSL

Outline

- Very-high-energy emission from SgrA*
- Radio-galaxies at very high energies
- Blazar variability at high energies

AGN population at VHE (>~100 GeV)

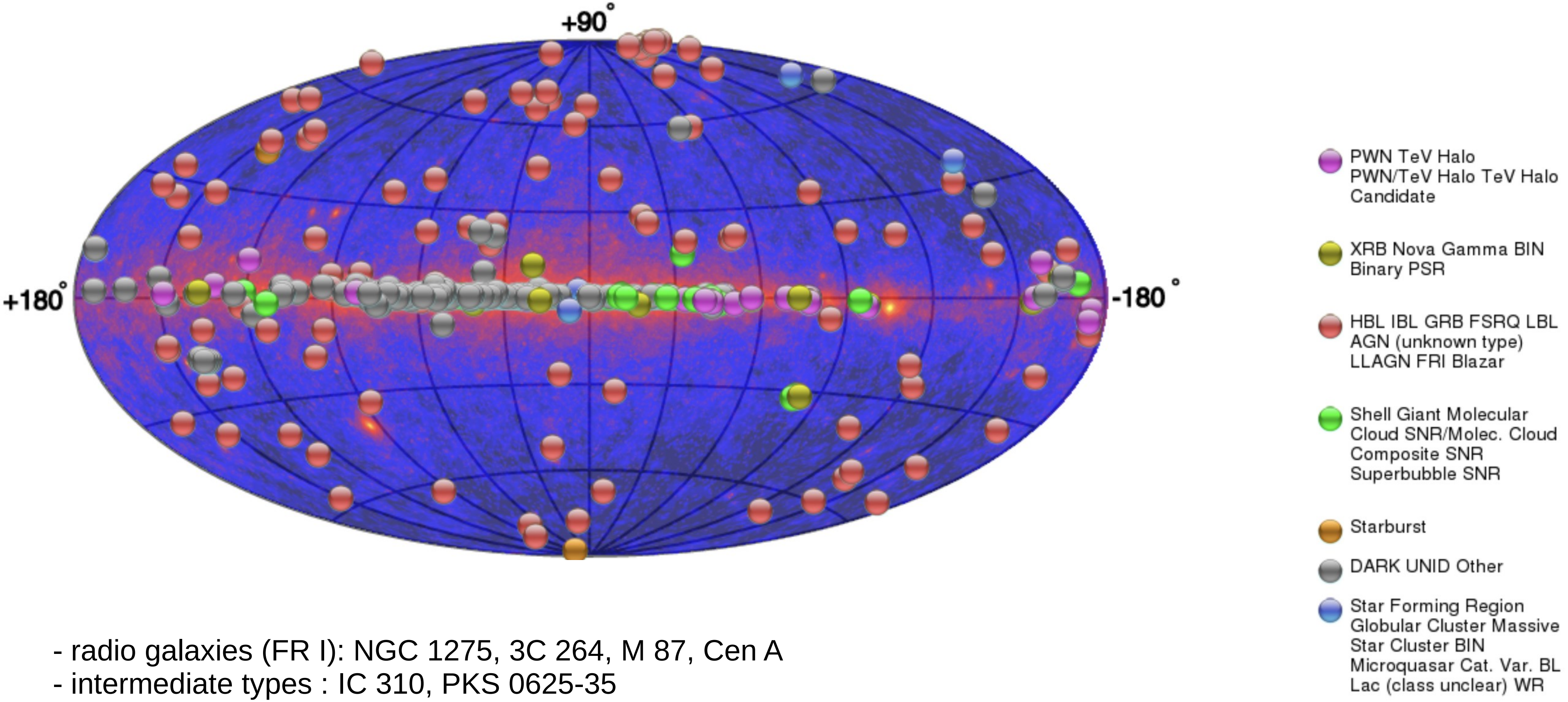

- radio galaxies (FR I): NGC 1275, 3C 264, M 87, Cen A
- intermediate types : IC 310, PKS 0625-35
- 82 blazars (FSRQ, LBL, IBL, HBL)
- 1 LINER ? (NGC 4278, LHAASO counterpart)

Very high energy emission from SgrA*

Detection of VHE gamma-rays with H.E.S.S.

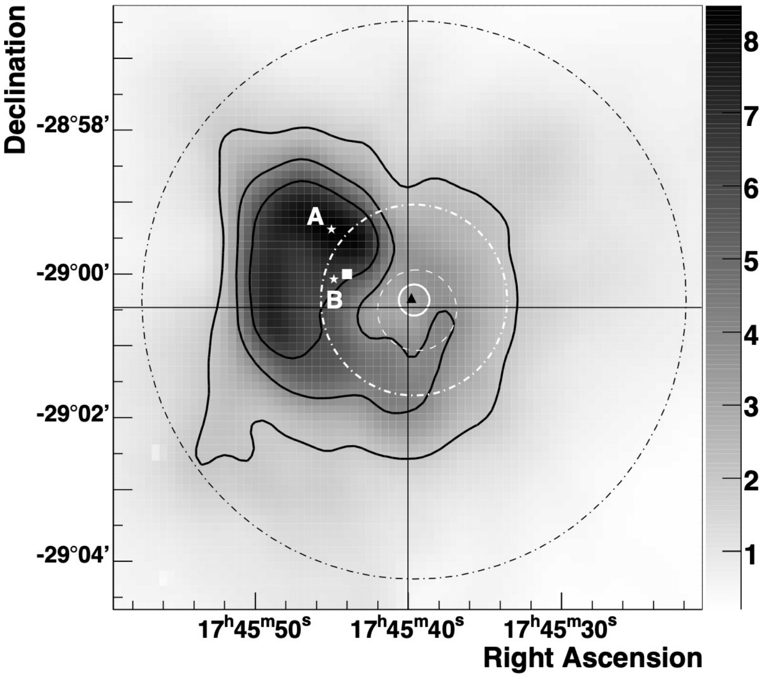

radio contours from VLA around the SNR Sgr A East (square);
Sgr A* shown by crosshair;
G 359.95-0.04 by triangle;
white circle : 68% CL total error contour of the best-fit centroid position of HESS

The point-like TeV source HESS J1745-290 coincides with the position of Sgr A* in the Galactic Center, but also with the pulsar wind nebula G 359.95-0.04
(angular resolution ~4' for 68% containment radius, pointing precision ~13'' for 68% containment radius).

No variability is seen from HESS J1745-290.
Consistent detections later on with MAGIC and VERITAS.

A more precise picture should emerge from observations with the future CTAO (angular resolution ~1', poiting precision <10'').

H.E.S.S. collaboration, F. Acero et al.
MNRAS 402 (2010) 1877-1882

Detection of a PeVatron with H.E.S.S.

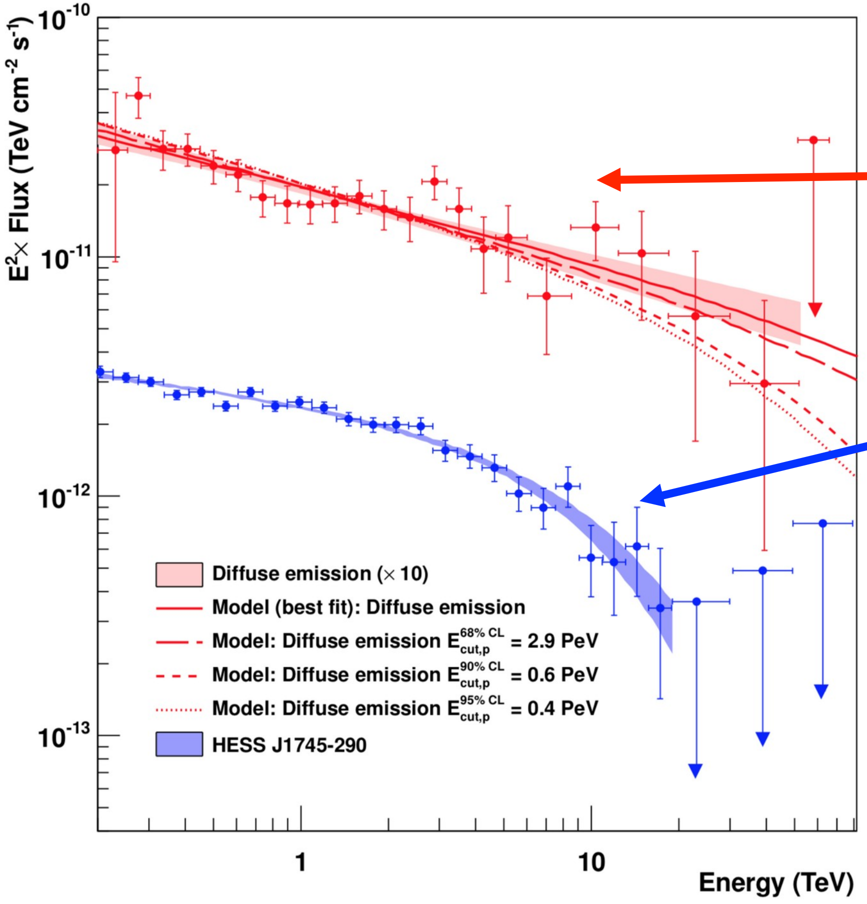

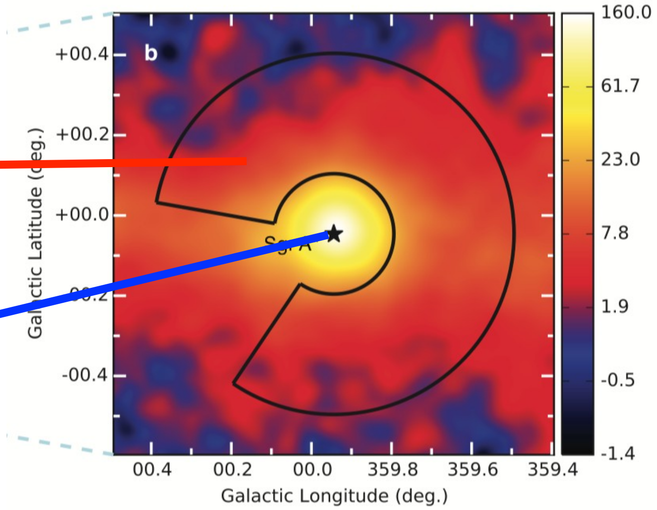

H.E.S.S. collaboration, Abramowski et al., Nature 531, 476-479 (2016)

In addition to emission from the point source HESS J1745-290, there is a diffuse emission component that is traced back to PeV cosmic rays (proton-proton collisions in central molecular zone).

-> First detection of a PeVatron coincident with the position of Sgr A*.

Prospects for CTAO : better resolution, higher energy range up to ~ 300 TeV.

Detection of a PeVatron with H.E.S.S.

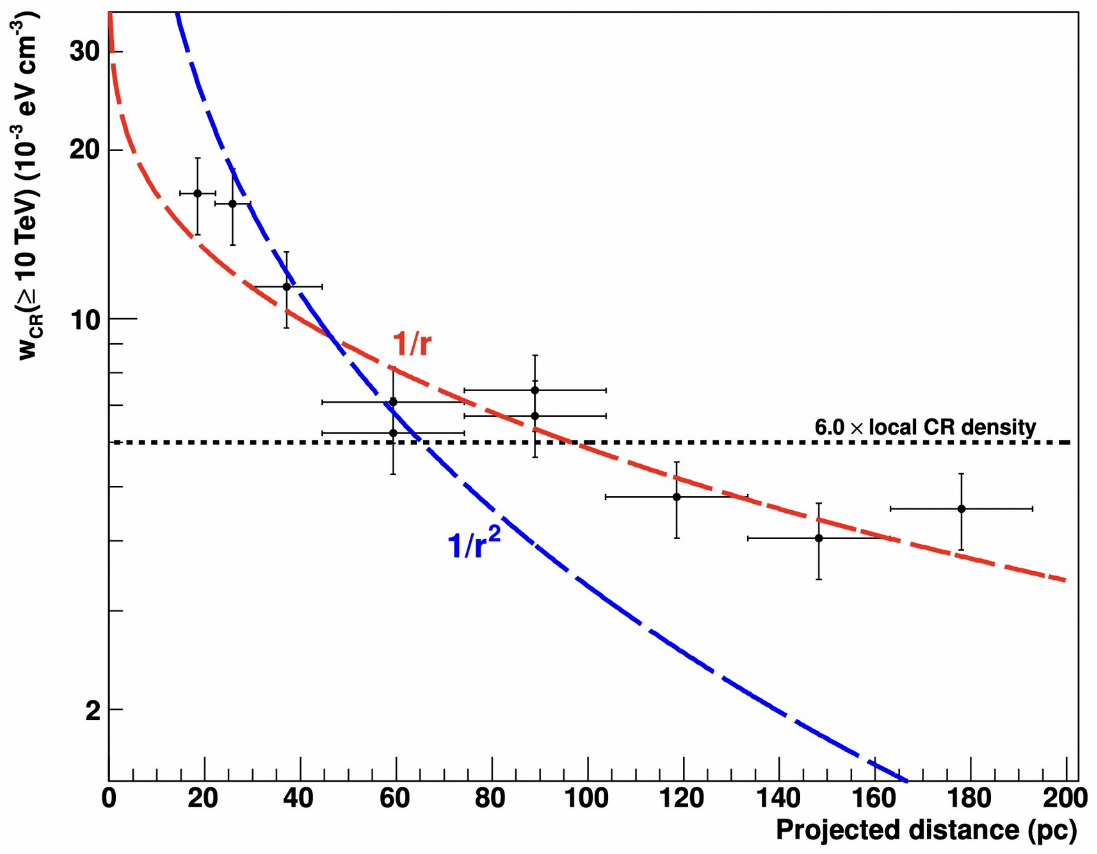

- Diffuse emission consistent with 1/r profile of the cosmic-ray density up to 200 pc

→ quasi-continuous injection of protons into the central molecular zone from a centrally located accelerator on a timescale
$\Delta t \geq t_{diff} \approx 2 \times 10^3 (D/10^{30}\ cm^2 s^{-1})^{-1}$ yr,
with D the diffusion coefficient for multi-TeV cosmic rays in the Galactic Disk.

(*H.E.S.S. Collaboration*)

- this accelerator alone can account for most of the flux of Galactic CRs around the "knee" if its power over the last ~10^6 years has been maintained at an average level of 10^{39} erg/s (→ past activity of SgrA* ?)

- escape of particles into the Galactic halo and their subsequent interactions with the surrounding gas can be responsible for the sub-PeV neutrinos recently reported by the IceCube collaboration

(cf. *F. Aharonian, Gamma 2024 conference*)

UHE gamma-rays detected with HAWC

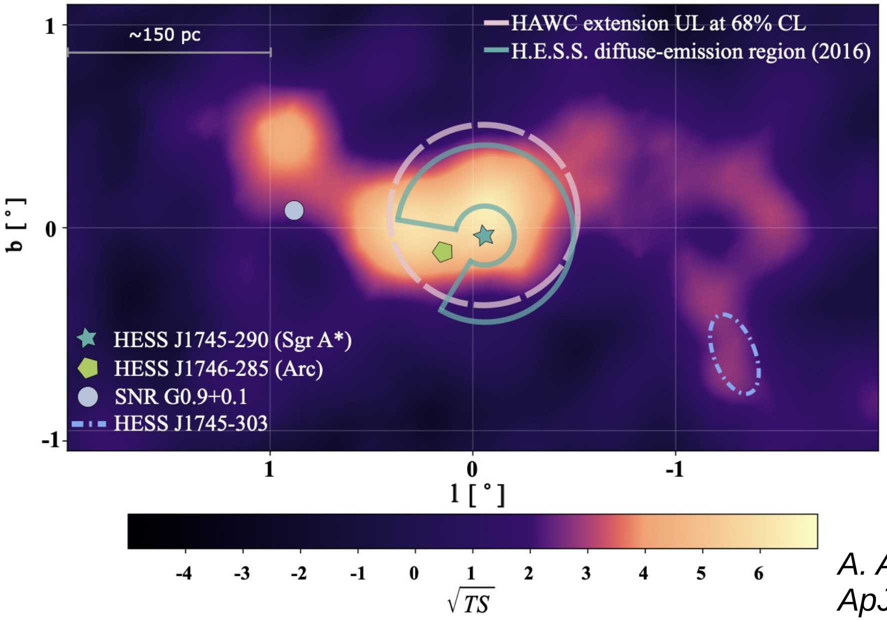

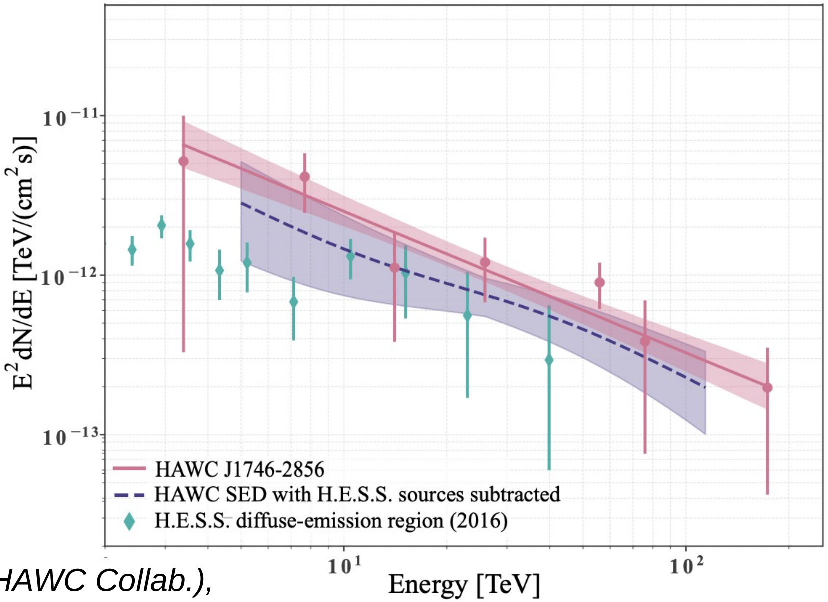

A. Albert et al. (HAWC Collab.), ApJL 973, 1 (2024)

- First detection of >100 TeV gamma rays from the GC region with a number of nearly 100 events. Strongly disfavours a purely leptonic accelerator.

- “We calculate the gamma-ray luminosity of the PeVatron and find that the cosmic-ray energy density is above the average, which clearly suggests the presence of freshly accelerated 0.1–1 PeV protons in the GC region.”

- several potential sites of proton acceleration within the emission region : vicinity of Sgr A$*$ (*H.E.S.S. Collaboration 2016*), Arches and Quintuplet star clusters (*Aharonian et al. 2019*)

Hint of a spectral break ?

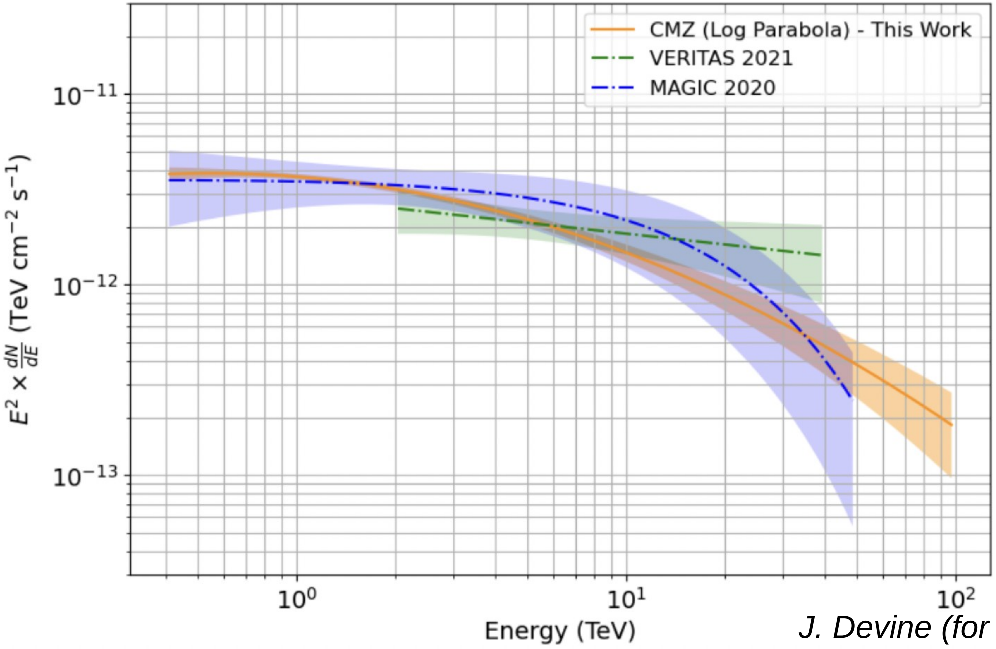

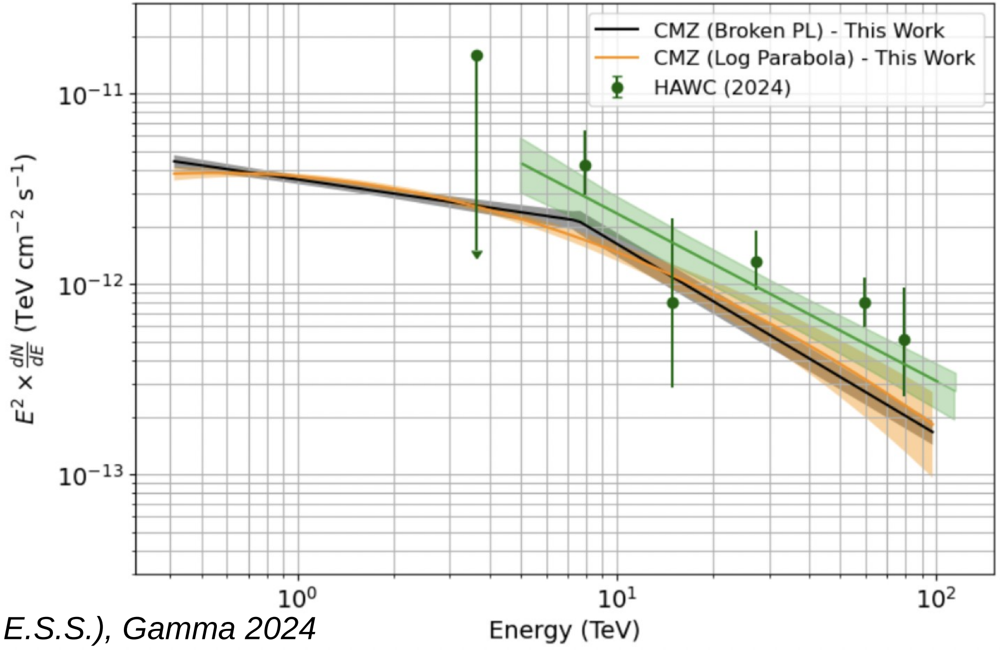

J. Devine (for H.E.S.S.), Gamma 2024

New analysis of H.E.S.S. data with detailed modeling of the central molecular zone (CMZ) :

- consistent with 2016 results, but indication of a spectral break / curvature

- origin : related to the accelerator itself ? To propagation effects ? To a contribution from multiple sources ?

(*J. Devin et al. for H.E.S.S., Gamma 2024 conference*)

Prospects for CTAO

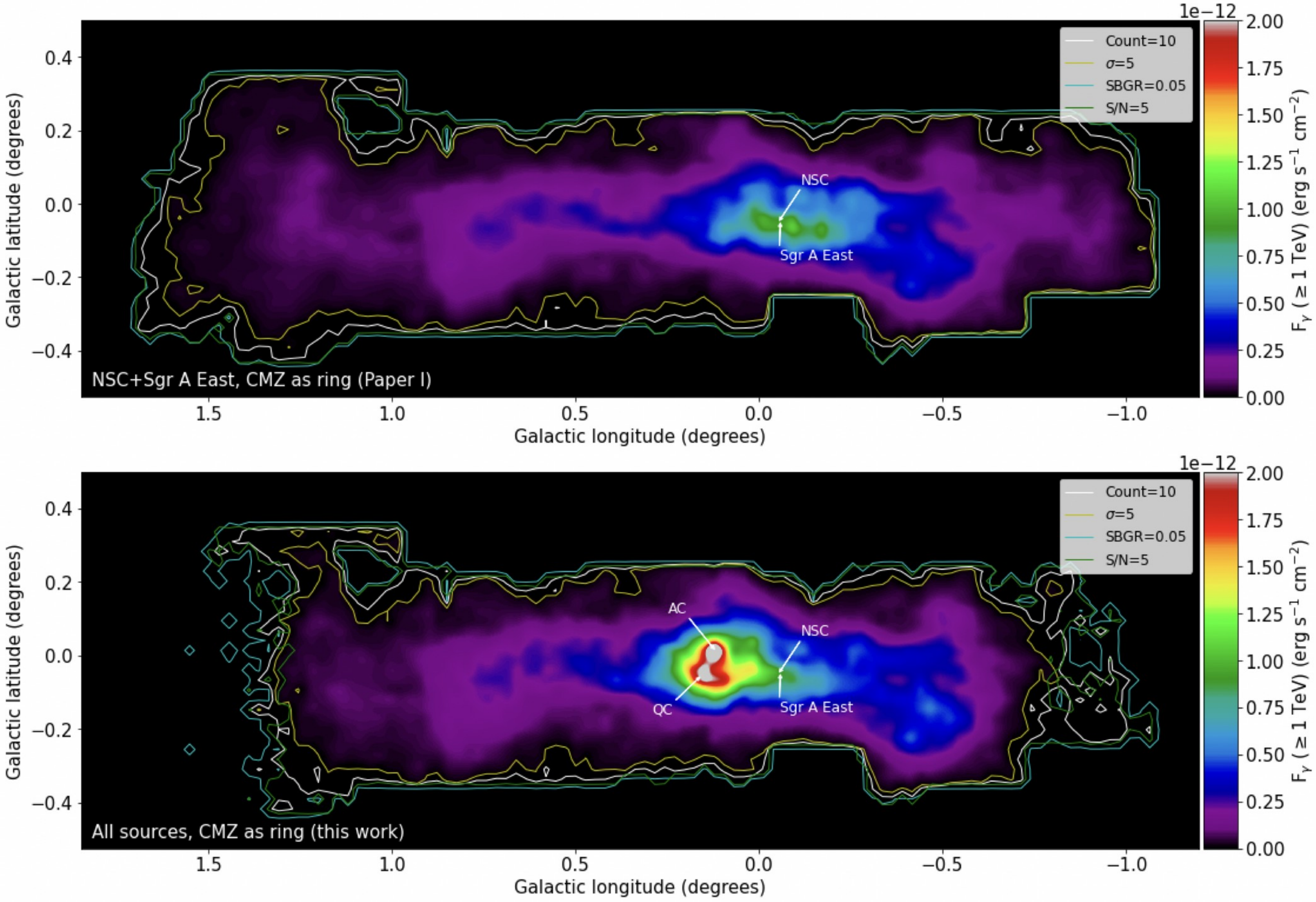

50h of observations with CTAO

A. Scherer, J. Cuadra, F.E.Bauer, A&A 679,114 (2023)

- To reproduce the existing observations detected by H.E.S.S., a ring-like gas distribution, with its mass set by the standard Galactic CO-to-H2 conversion factor, and CR acceleration and transport from all relevant sources are modelled.

- “ More realistic CR dynamics suggest that the CMZ has a large inner cavity and that the GC PeVatron is a composite CR population accelerated by the Arches, Quintuplet, and nuclear star clusters, and Sgr A East.”

-” CTA will be able to differentiate between models with different CR dynamics, proton sources, and CMZ morphologies, owing to its unprecedented sensitivity and angular resolution.”

→ Key Science Project for CTAO

Radio galaxies at very high energies

IC 310 : particle acceleration close to the SMBH ?

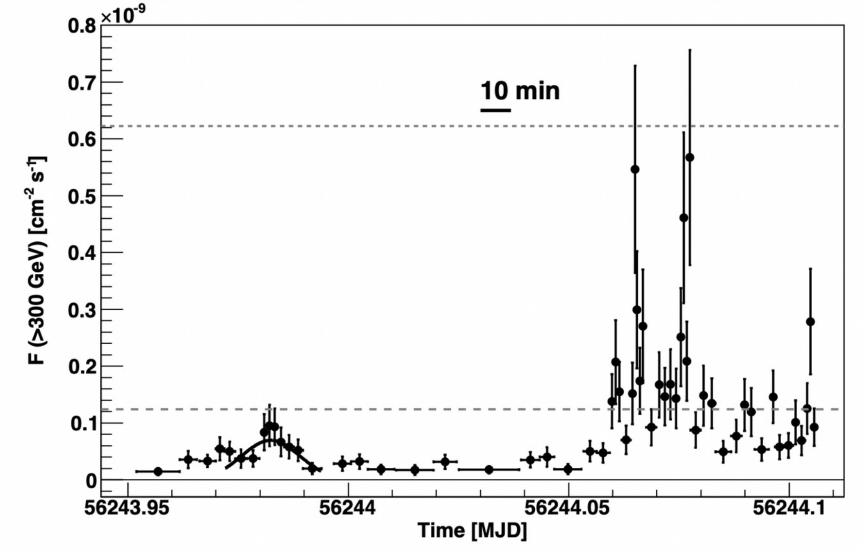

J. Aleksic et al., The MAGIC Collaboration, Science 346, 1080 (2014)

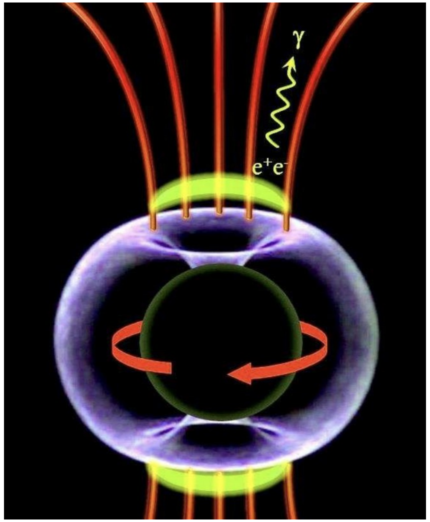

VHE observations with MAGIC show variability with doubling time scales dt < 5 min, implying an emission region < 0.2 r_G of the central BH. (Contrary to blazars, relativistic effects on dt expected to be small due to small $\delta < 6$.)

→ pulsar-like particle acceleration by the electric field across a magnetospheric gap above the ergosphere ?
Problem : VHE power of a (steady) gap of height h scales with the jet power :
$L_{VHE} \sim L_{jet} (h/r_g)^a$, a = 2 − 4 with $L_{jet} \sim 10^{43}$ erg s^{-1} → too low for observed VHE flux ? (*Rieger, Levinson 2018*)

→ other mechanisms : magnetic reconnection regions in the jet ? jet-cloud interactions in the jet ? …

2024 : renewed TeV flaring seen by Veritas, LHAASO !

Centaurus A : particle re-acceleration in the kpc jet

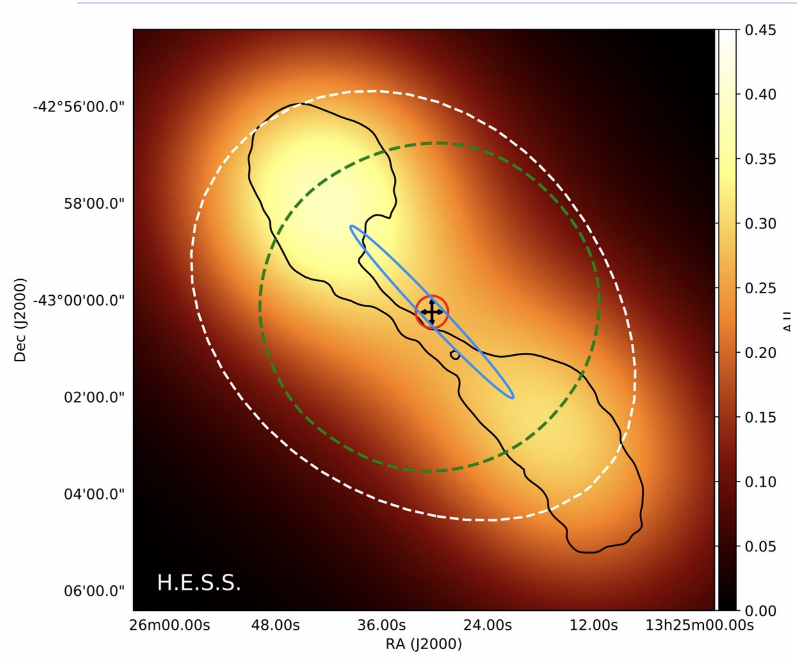

radio VLBI contours and map convolved with H.E.S.S. PSF ; blue : best-fit elliptical Gaussian, green : H.E.S.S. PSF , white : contour of 5σ excess

The H.E.S.S. Collaboration Nature 82, 356 359 (2020)

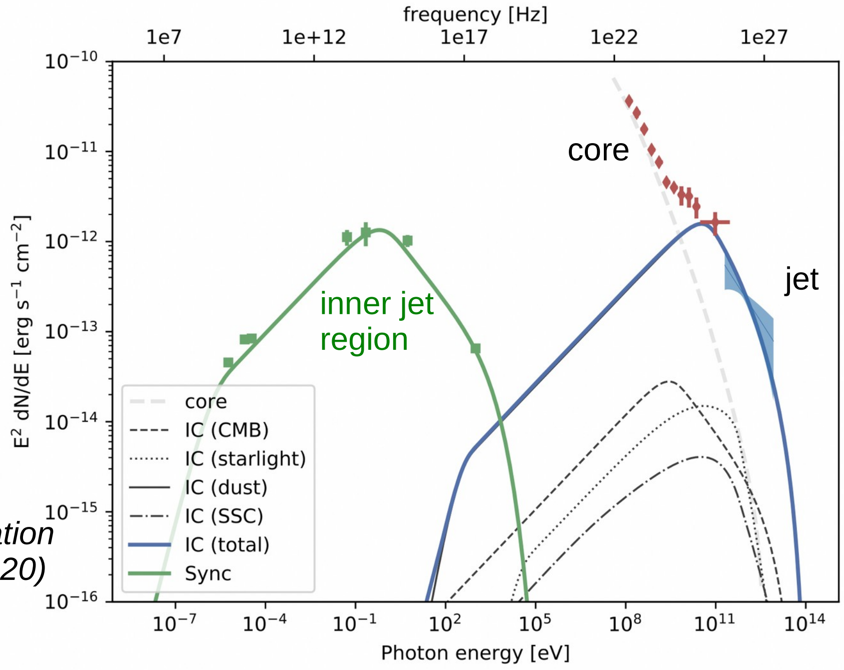

Extended VHE emission is seen from the kpc jets of Cen A, implying an efficient re-acceleration mechanism of particles at large distances from the jet base (stochastic ? shear ? shocks ? …)

VHE emission is ascribed to IC upscattering of mainly radiation from dust. Particle energies required with $\gamma \sim 10^7 - 10^8$!

→ Key Science Project for CTAO

M87 : the VLBI – high-energy connection

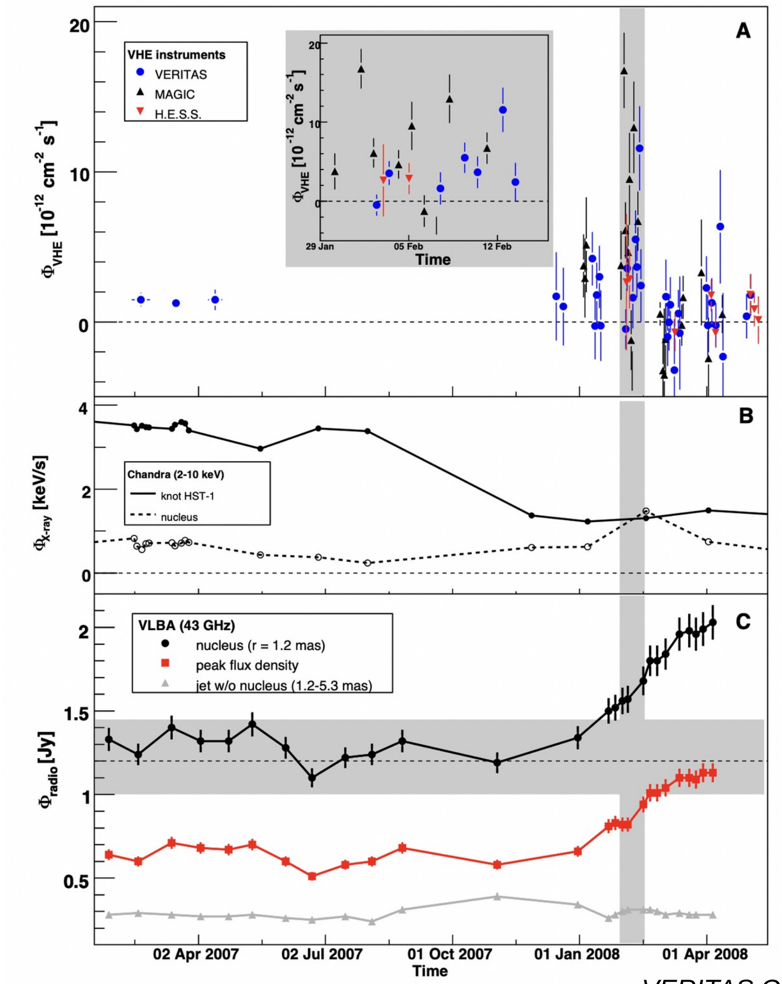

VERITAS Collab. et al. 2009

2008 VHE flare of the radio galaxy M87 :

Correlation with high activity (radio VLBI, X-rays) from the **nucleus** (radio core) and not from HST1.

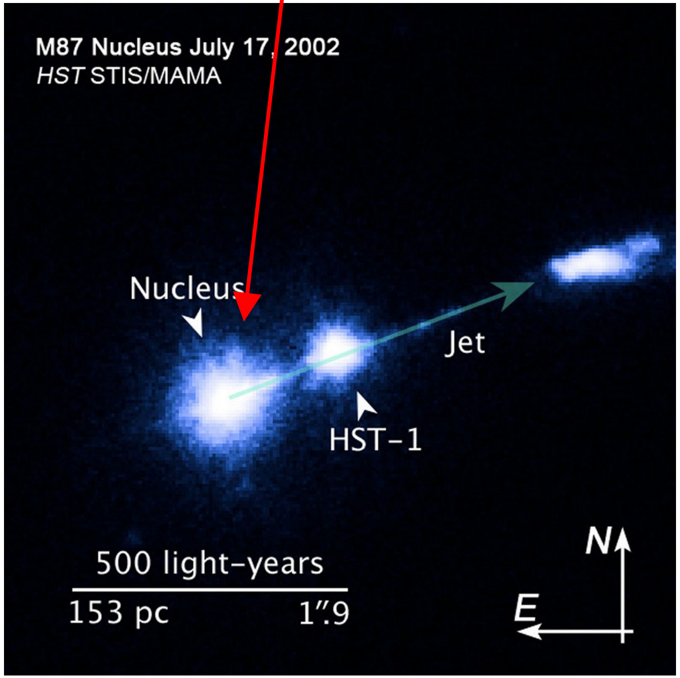

M87: the VLBI – high-energy connection

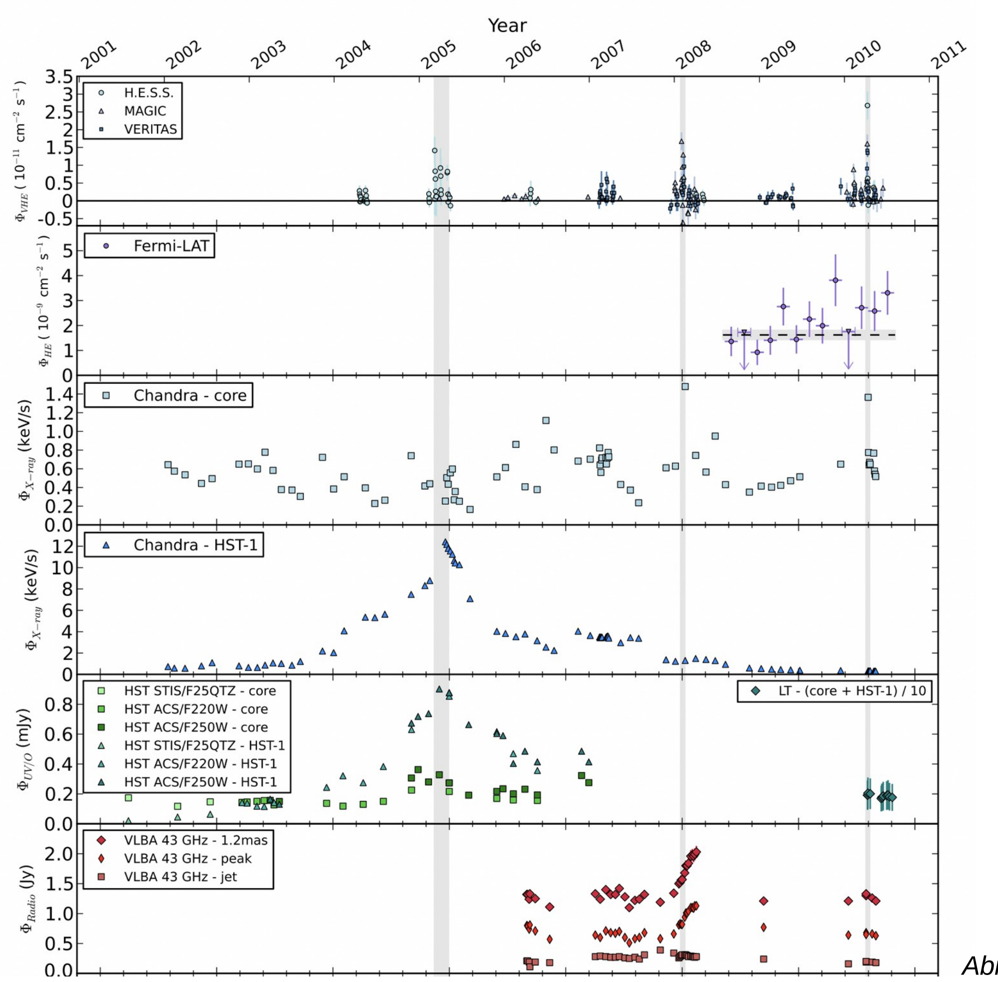

Abramowski. et al. 2012

BUT :

2005 VHE flare of the same source: Correlation with high activity (optical, X-rays) from the radio knot **HST1**.

Correlation of the **2010** VHE flares with the **nucleus**.

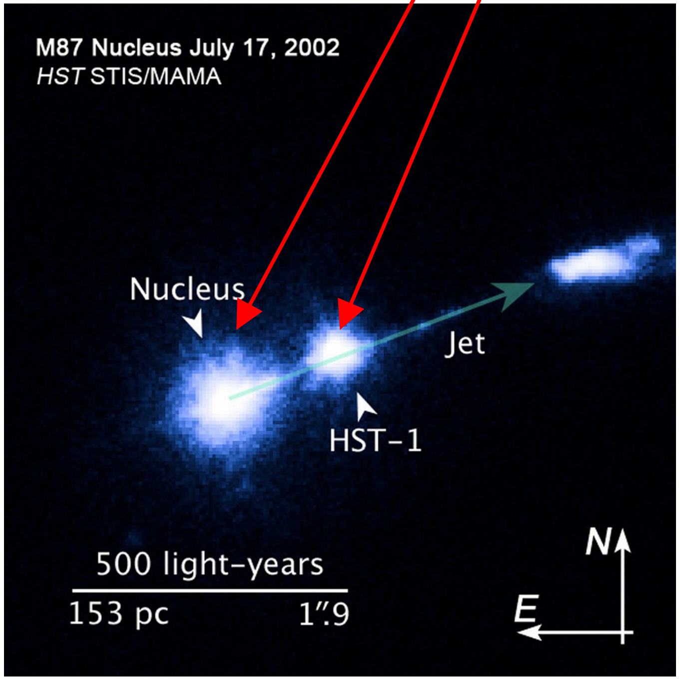

M87: the VLBI – high-energy connection

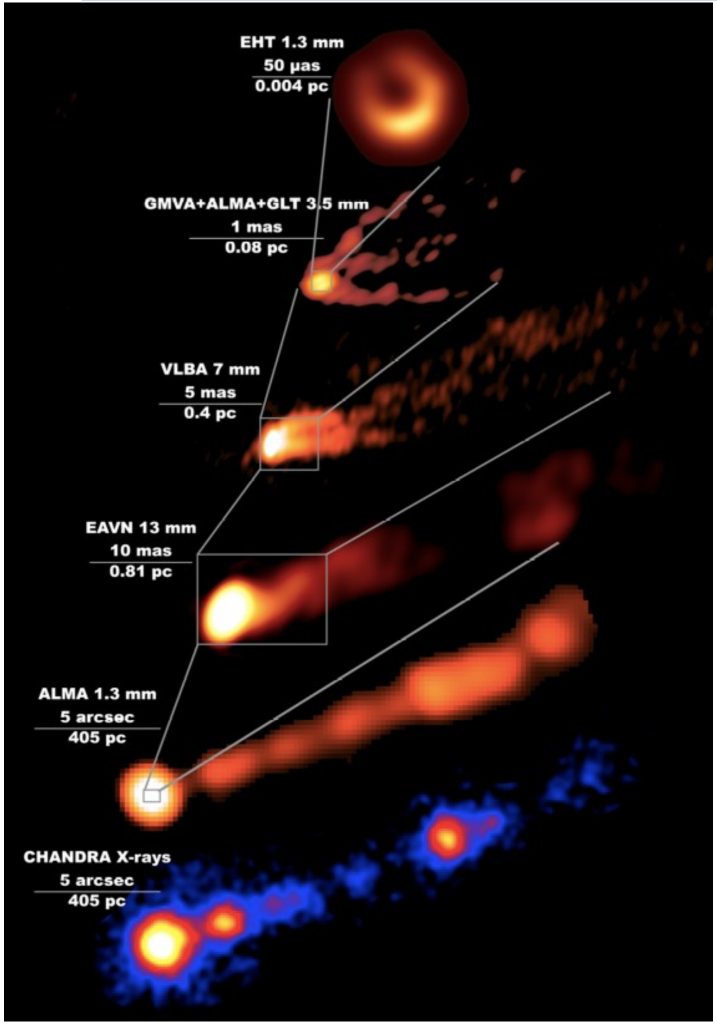

2018 : IACTs contributed to a new multi-wavelength observation campaign, including the Event Horizon Telescope.

Detection of the first very-high-energy flare since 2010, with flux-doubling time of ~36h. Consistent with Fermi flux; X-ray flux higher than 2017.

SED modelling with several scenarios with distinct low-energy and high-energy emission regions.
→ no clear constraint on the location of the VHE emission region.

J.C. Algaba et al. 2024

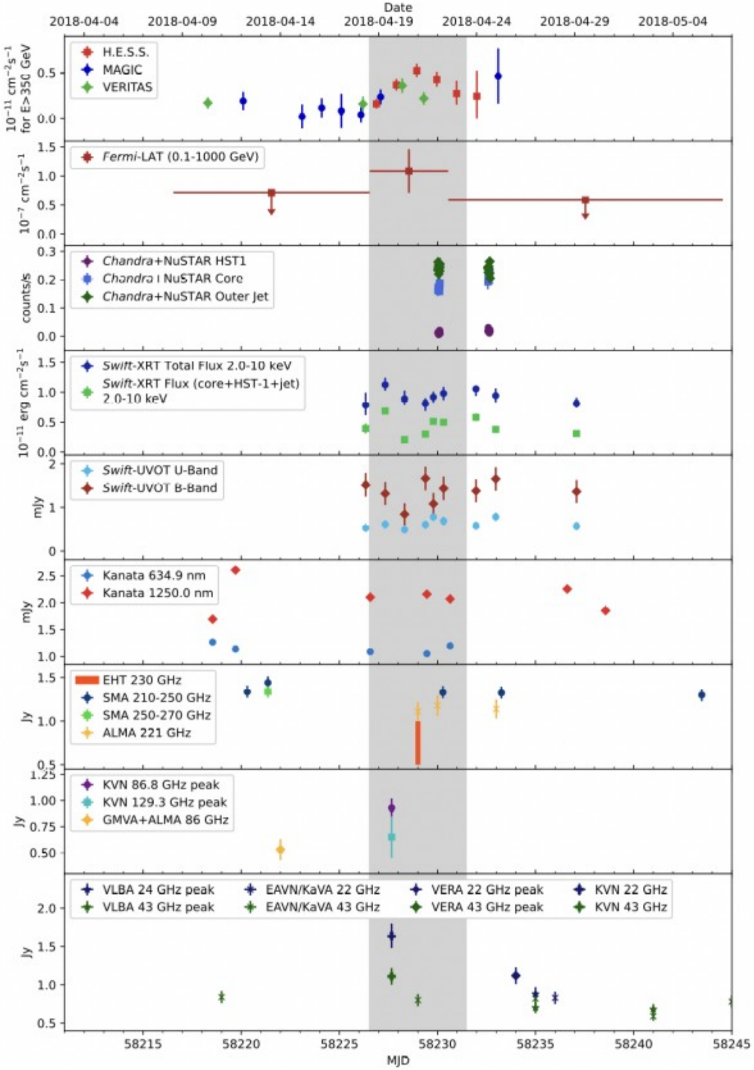

Blazar variability at high energies

ongoing work...

blazar emission in the leptonic model

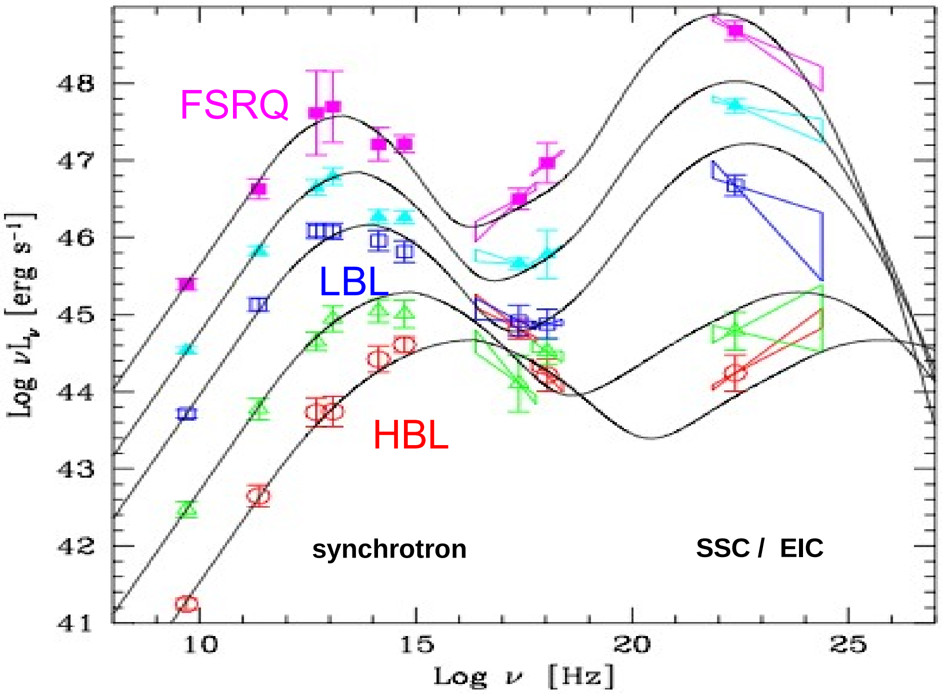

Donato et al. (2002), based on Fossati et al. (1998)

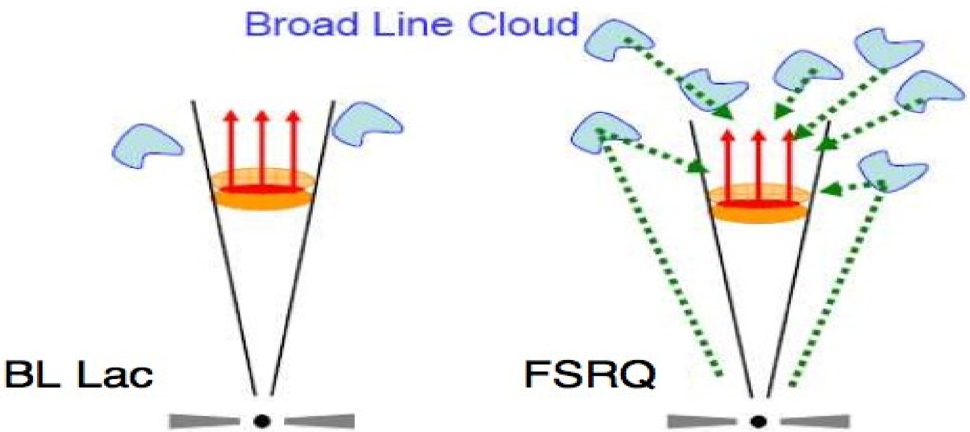

B. Lott, Cospar 02/10

- Disk and Broad Line Region emit weakly

- γ-rays due to **Synchrotron Self Compton**

- Disk and Broad Line Region emit strongly

- γ-rays mostly due to **External Inverse Compton** → high Compton dominance

luminous **FSRQs** with high peaks in gamma band ↔ less luminous **BL Lac objects** with lower peaks in gamma band

variation of the parameters of the emission region

a case study

(work with S. Le Bihan, A. Dmytriiev 2024;
cf. Proceedings of Gamma 2024 Conf.)

an orphan flare from 3C 279 in 2013 ?

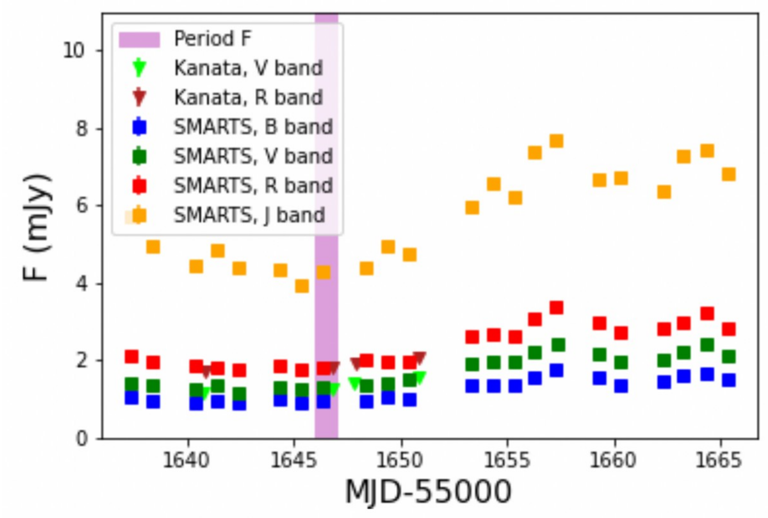

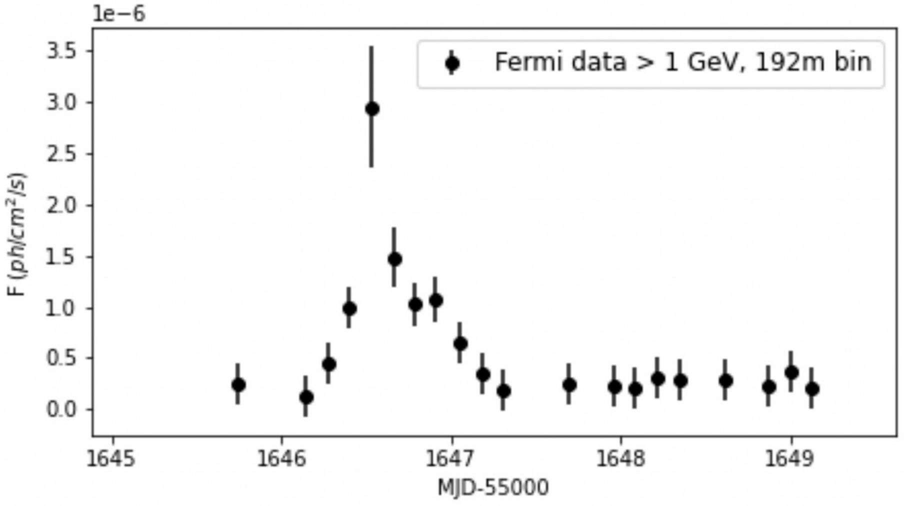

Bihan 2024;
with data from Hayashida et al. 2015

- significant Fermi flare from this FSRQ on 20.12.2013

- no significant variability in simultaneous optical data

- no simultaneous X-ray data

the model : BLR

- External Compton emission dominated by the photon field from the Broad Line Region

- photons from a spectrum of emission lines

- BLR modelled as a spherical shell with inner radius $R_{BLR} \sim 3 \times 10^{17}$ cm (0.1 pc)

- For distance $d > R_{BLR}$, the energy density decreases as :

$$U'(\epsilon', d) = \frac{L'_{BLR}(\epsilon')\Gamma^2_{blob}}{3\pi R^2_{BLR}\, c\left(1+(d/R_{BLR})^{\beta_{BLR}}\right)}$$

(Hayashida et al 2012)

- index β_{BLR} set to 4

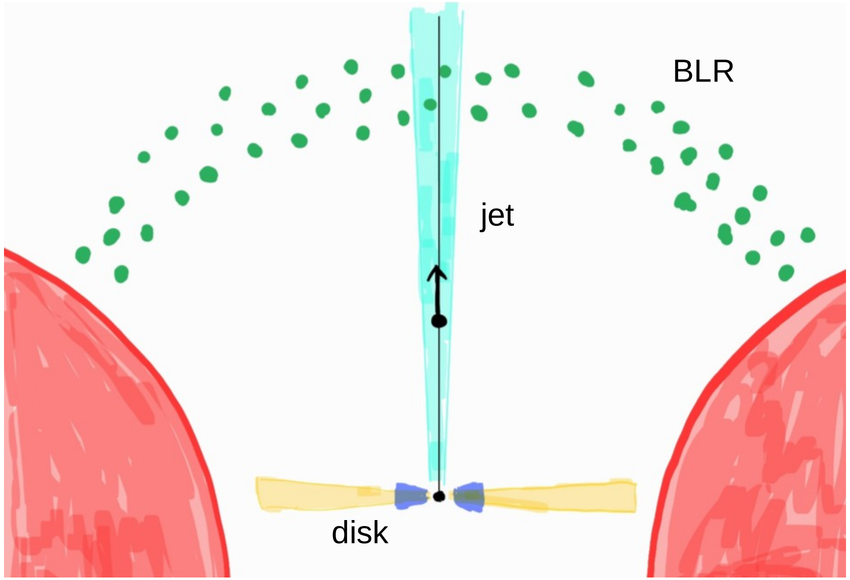

dust
torus

the model : stationary + accelerating blobs

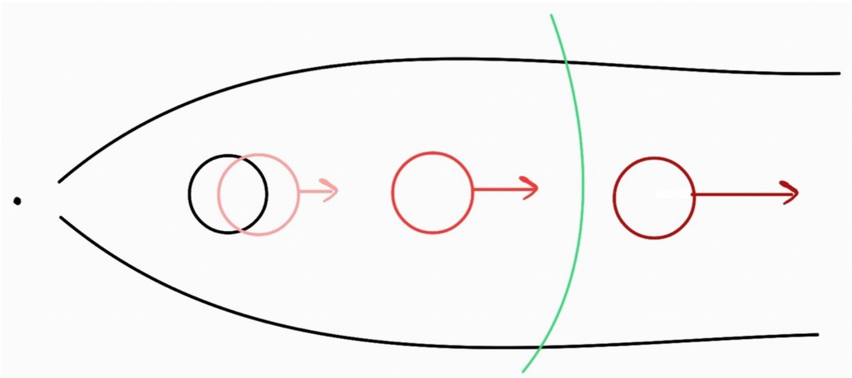

low-state emission from a stationary emission region at the base of the jet ("**blob 1**")

flare is caused by an accelerating, expanding emission region ("**blob 2**") (differential collimation) :

$$\Gamma_{blob} = min\left(\Gamma_{max}, \sqrt{d/(3R_s)}\right)$$

(Ghisellini & Tavecchio 2009)

$\Gamma_{max} = 30$
→ acceleration up to $d_{max} = 4 \times 10^{17}$ cm

- for $d < R_{BLR}$, as blob 2 accelerates :

$$U' \propto d$$

- for $d > d_{max}$, as blob 2 advances at constant velocity :

$$U' \propto d^{-\beta_{BLR}}$$

- particle spectrum from injection of a steep power-law + cooling (incl. adiabatic) + particle escape

- B'_{blob1} = 3.2 G , $R'_{blob1} \sim 3 \times 10^{15}$ cm, initial B'_{blob1} = 0.01 G , initial $R'_{blob2} \sim 2 \times 10^{16}$ cm

model vs. data

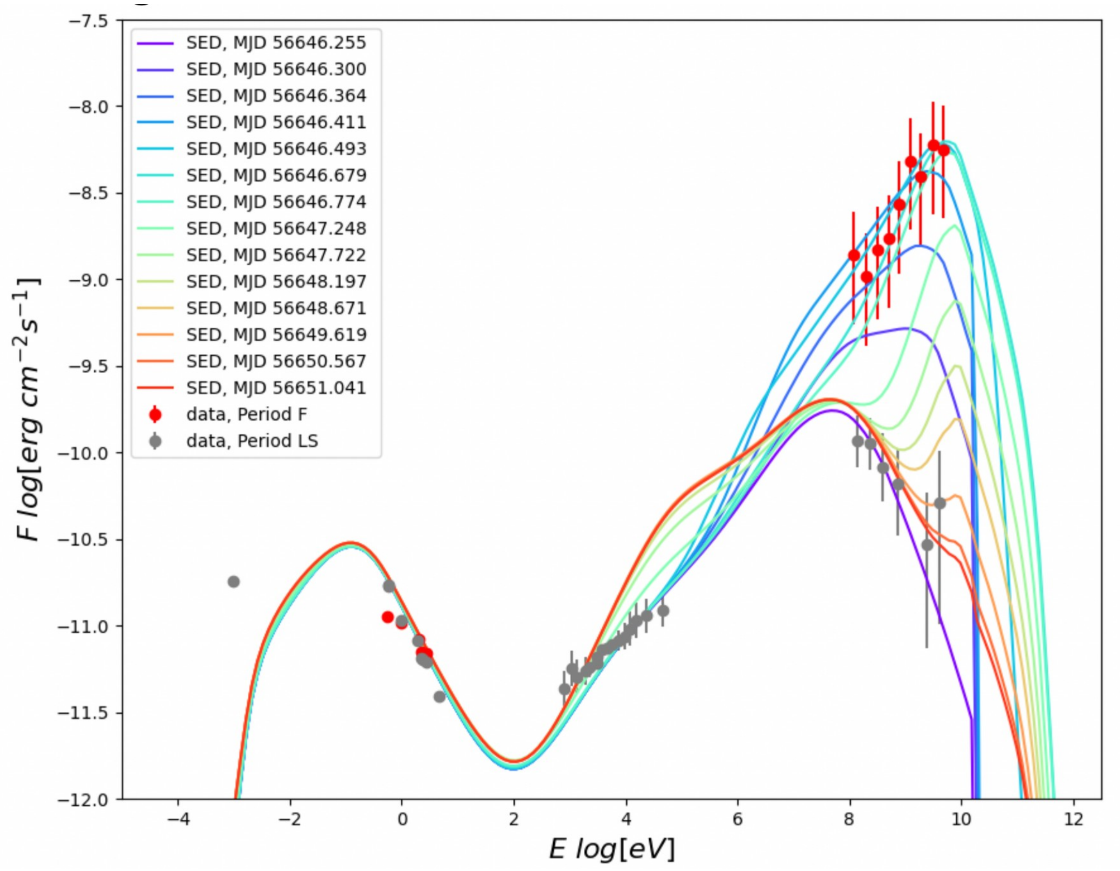

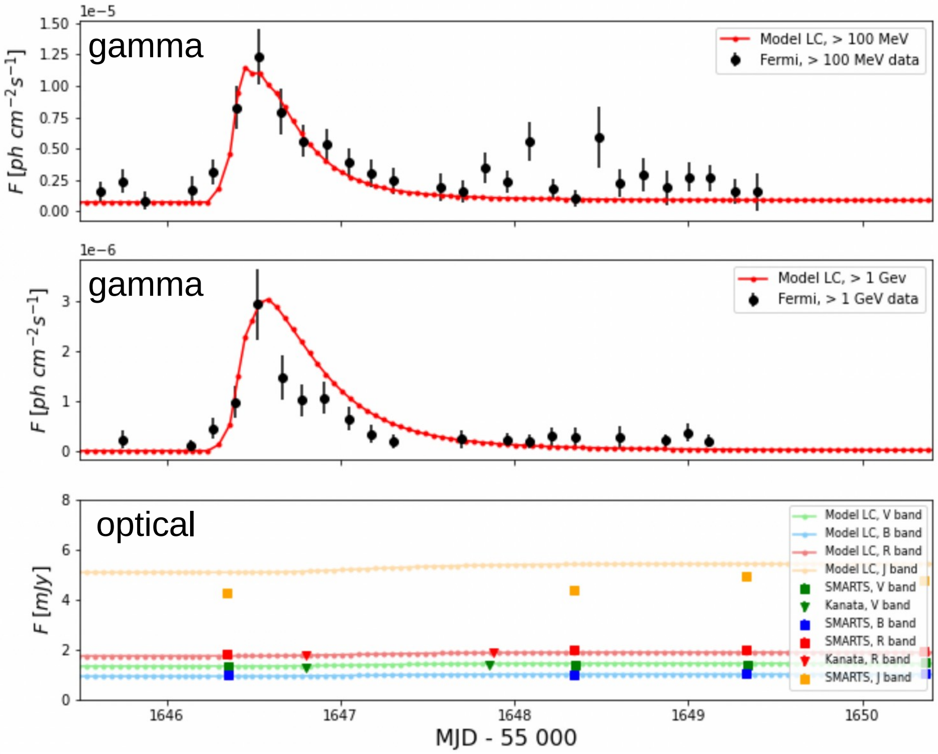

variation of the particle distribution

a systematic study

(work with P. Thevenet, C. Boisson, A. Dmytriiev 2023/2024;
publication to be submitted)

example : Fermi-I acceleration

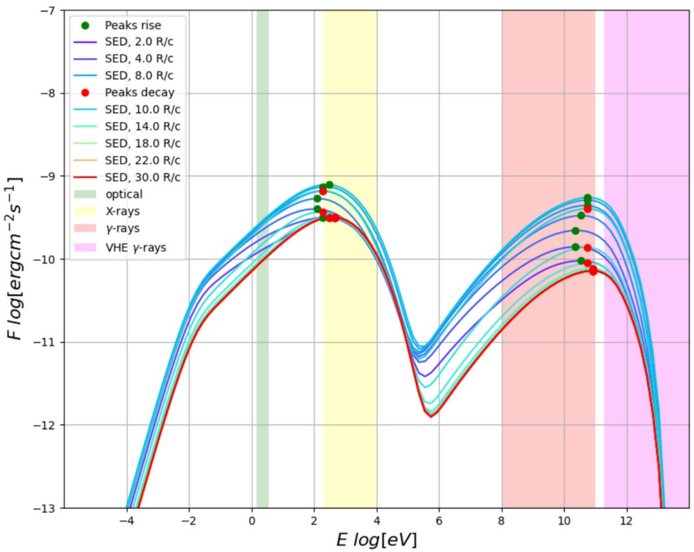

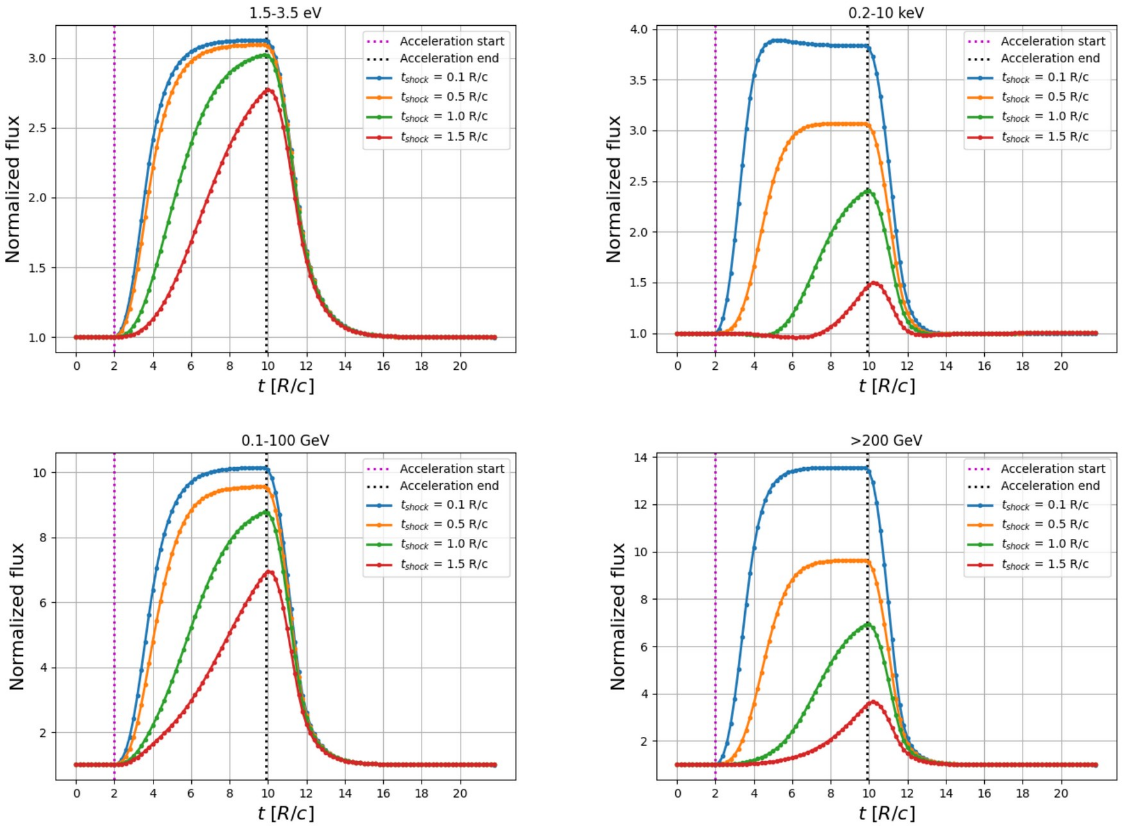

- shift of peaks during flare

- flare onset shifts between energy bands

- occurrence of a “plateau” in light curves only for very rapid t_{shock}

example: Fermi-II re-acceleration

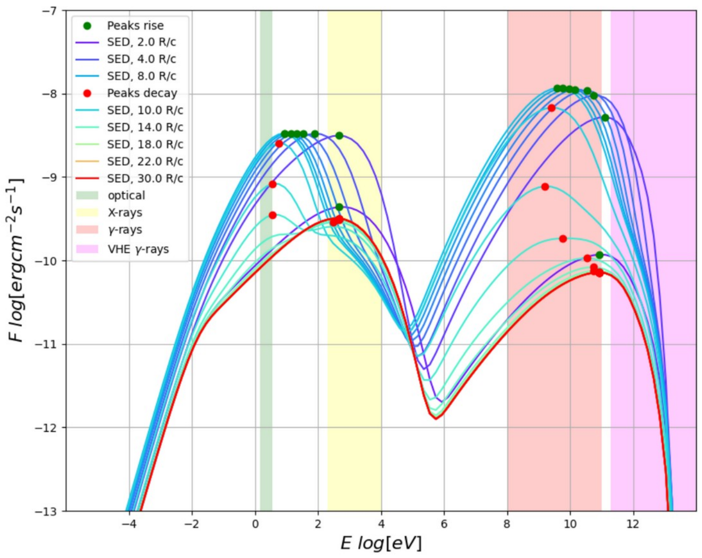

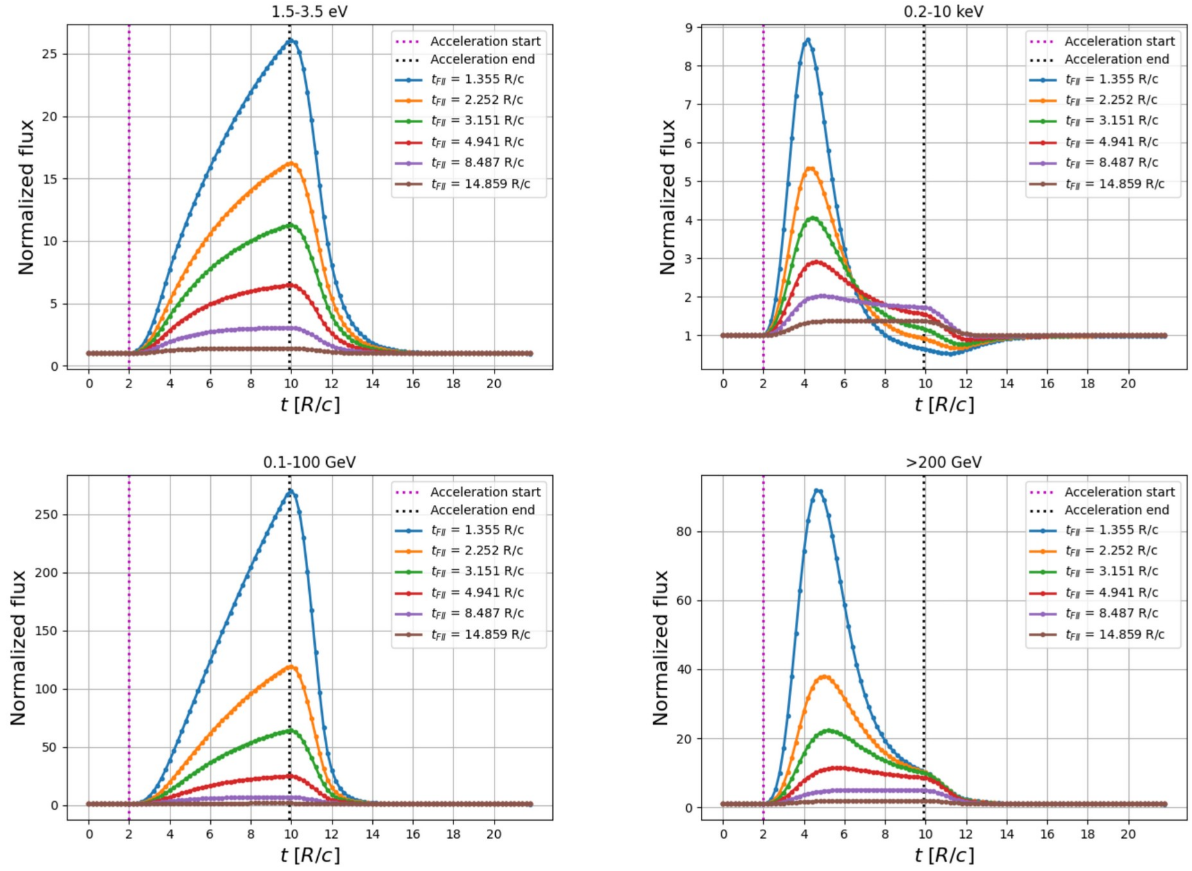

- strong shift of peaks during flare
  → hysteresis

- Compton dominance > 1 for very rapid t_{FII}

- strong energy dependant time delays between light curves for very rapid t_{FII}

application to a flare of Mrk 421

First application to a 2013 flare from Mrk 421 (BL Lac object) to illustrate the light-curve shapes of different scenarios :

- none of the generic scenarios provides a satisfactory representation of the data
  → very difficult to get the fluxes right between energy bands without fine-tuning injection rate and spectral index

- time delays of the peak flux can appear even between neighbouring energy bands

→ a full representation of SED and light curves might require a combination of scenarios & automated fitting procedure

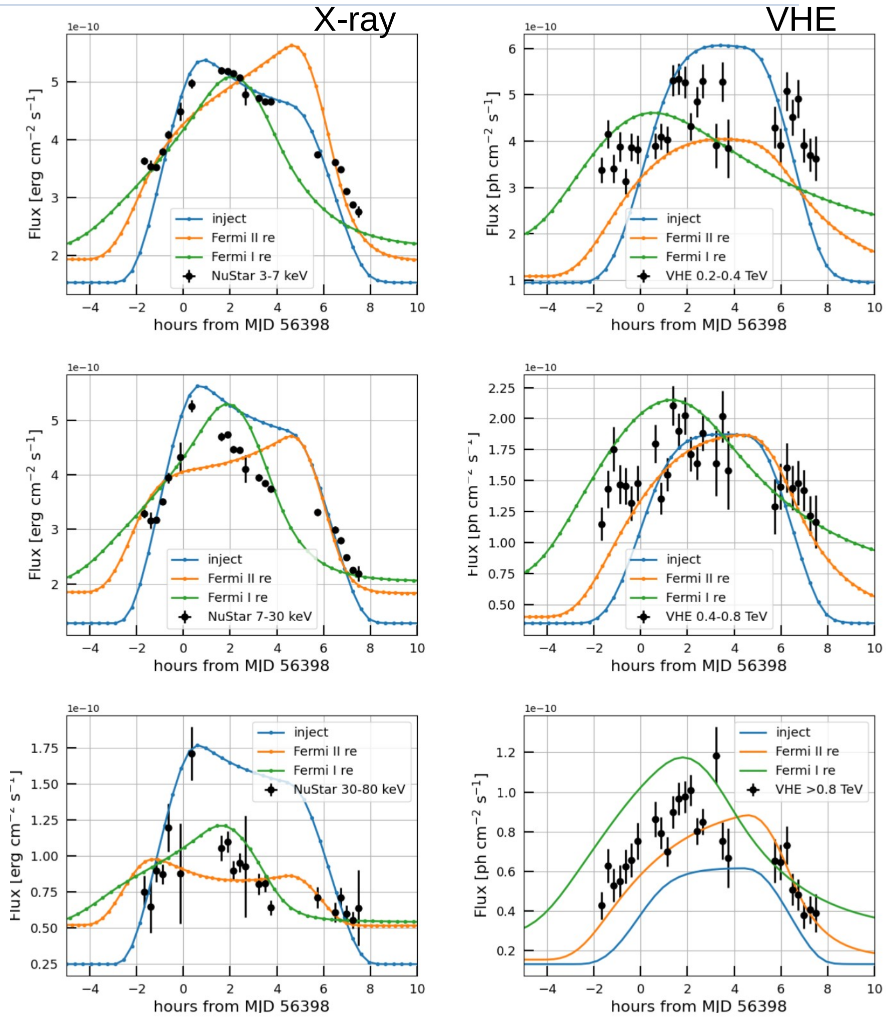

Outlook

Possible synergies with Gravity+ (?) :

- Sgr A* , nearby radio galaxies , blazars :

explore / constrain cosmic-ray acceleration scenarios near the SMBH ?
(magnetosphere , jet base , accretion flow , disk wind ...)

explore a possible origin of variability near the SMBH ?

- Flat-Spectrum radio quasars :

improve our models of the Broad Line Region with observational constraints on the extension, geometry, profile ?

particle evolution in the EMBLEM code

Cooling terms   Acceleration terms

$$\frac{\partial N_e(\gamma,t)}{\partial t} = \frac{\partial}{\partial \gamma}\left[\left(b_c(\gamma,t)\gamma^2 + \frac{1}{t_{ad}}\gamma - a(t)\gamma - \frac{2}{\gamma}D_{F_{II}}(\gamma,t)\right)N_e(\gamma,t)\right] + \frac{\partial}{\partial \gamma}\left(D_{F_{II}}(\gamma,t)\frac{\partial N_e(\gamma,t)}{\partial \gamma}\right) - N_e(\gamma,t)\left(\frac{1}{t_{esc}} + \frac{3}{t_{ad}}\right) + \dot{Q}_{inj}(\gamma,t)$$

Injection term

Cooling

- Synchrotron and Inverse Compton: $b_c(\gamma,t)$
- Adiabatic expansion: $t_{ad}(t) = \frac{R(t)}{\beta_{exp}c}$
- Escape: $t_{esc}^{(turb)} = \left(\frac{R}{c}\right)^2\left(\frac{\delta B}{B}\right)^2\frac{c}{\lambda_{max}}\left(\frac{r_L}{\lambda_{max}}\right)^{q-2}$

Acceleration

- Fermi I: $a = 1/t_{shock}$, $\dot{Q}(\gamma,t)$
- Fermi II: $D_{F_{II}}(\gamma,t) = \frac{p^2}{t_{F_{II}}}$

$$t_{F_{II}} = \frac{1}{\beta_A^2}\left(\frac{\delta B}{B}\right)^{-2}\frac{\lambda_{max}}{c}\left(\frac{r_L}{\lambda_{max}}\right)^{2-q}$$

the model : low state

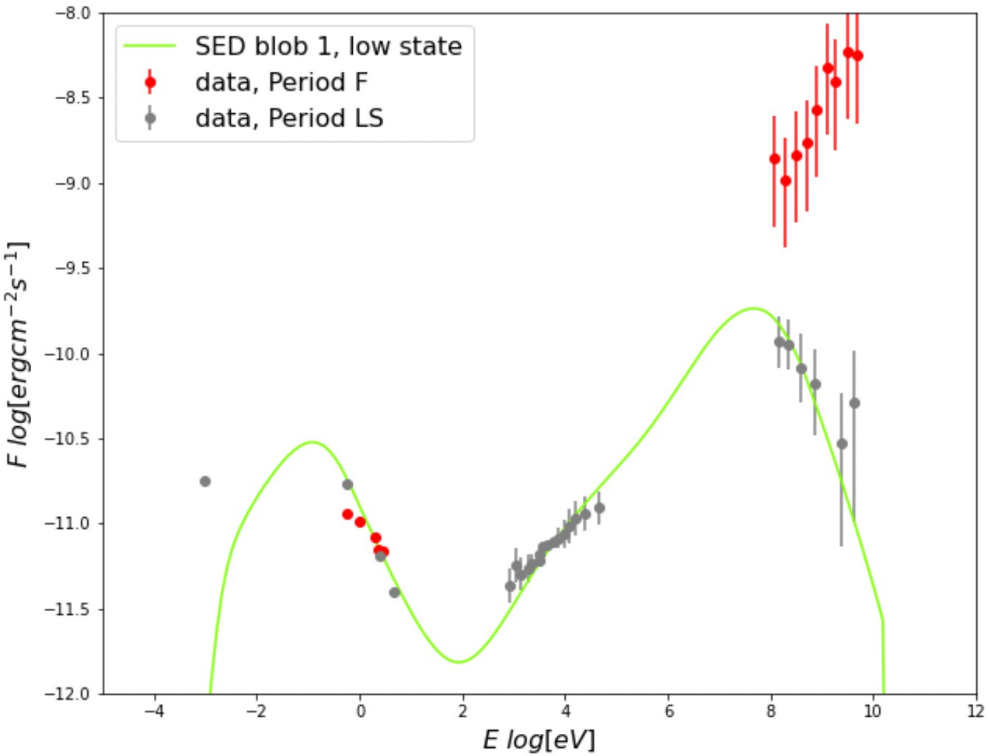

- time-dependent leptonic model EMBLEM including external photon fields (disk, BLR, dust torus)

- continuous emission during low state modelled with single stationary emission region (“blob 1”)

- steady-state spectrum from injection of a steep power-law + cooling + particle escape

- B’ = 2.5 G , Doppler factor ~ 19 , R'_{blob1} ~ 2 x 10^{16} cm , distance from black hole : d_1 ~ 5 x 10^{16} cm

the scenarios

injection

Q_{inj} : fixed injection rate, fixed PL spectrum, injected during flare window

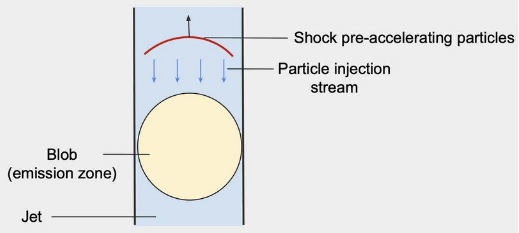

Fermi-I acceleration

Q_{inj} with increasing γ_{max} during flare window

t_{FI} : time-scale of γ_{max} evolution

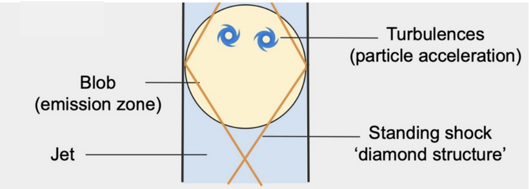

Fermi-I re-acceleration

Q_{inj} : fixed continuous PL injection

t_{shock} : time-scale for sys. energy gain

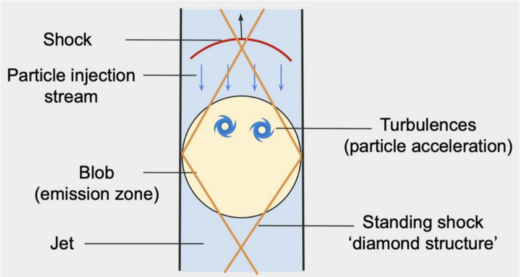

injection & adiabatic expansion

Q_{inj} plus fixed expansion rate

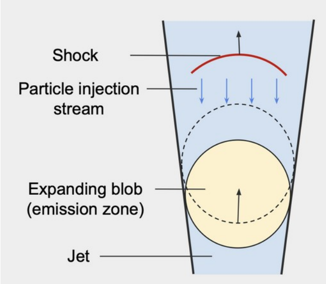

Fermi-II acceleration

injection of cold particles

t_{FII} : acceleration time scale

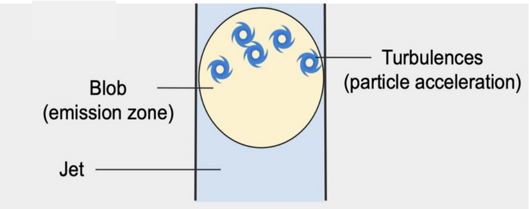

Fermi-II re-acceleration

Q_{inj} : fixed continuous PL injection

t_{FII} : acceleration time-scale

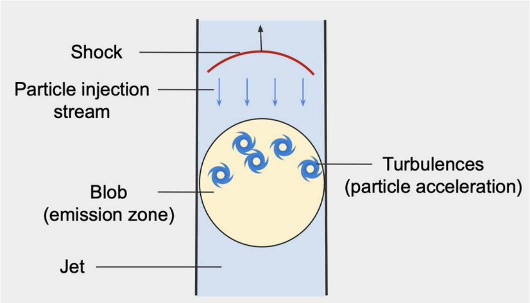

light-curve comparison

Even for a single emission region, a large variety of flare shapes !

• **injection** scenarios : onset of the flare rise occurs at the same time in all bands. Occurence of plateaux.

• **Fermi-I** scenarios : flare onset is delayed at higher energies.

• **Fermi-II** scenarios : flare onset occurs ~ at the same time in different bands. Acceleration of cold particles does not reach a plateau. Efficient re-acceleration leads to a flare that is peaking earlier at higher energies.

Decay times determined by the escape time and the effect of radiative cooling.

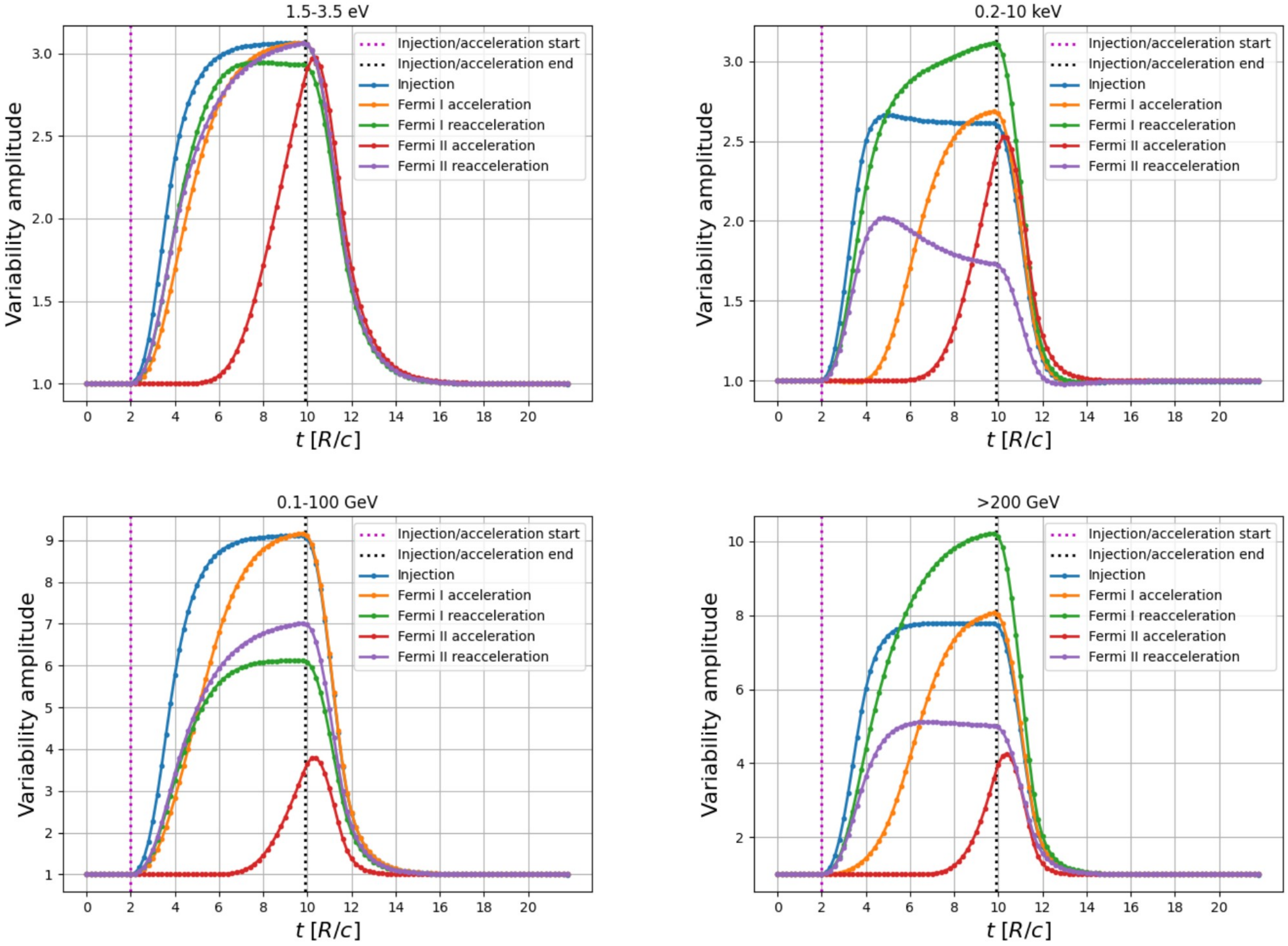

physical origin of flares

1) variation of the macroscopic parameters of the emission region

- change in size of emission region R → particle density, magnetic field B (expansion, contraction)

- change in magnetic field B or external radiation field

- change in Doppler beaming (Lorentz factor, viewing angle)

2) variation in the energy distribution of the emitting particles

- particle injection (pre-accelerated particle distribution)

- particle acceleration (shock, turbulence, shear, magnetic reconnection)

first conclusions

The good overall agreement between model and data suggests that our scenario of an accelerating blob can explain orphan flares from FSRQs without any variation of the particle distribution.

In this scenario, the **flare decrease** reflects the **BLR density profile**.

Issues with our parameters requiring further scrutiny :

- large difference between the magnetic field strengths assumed for blob1 and blob2

- modelling of stationary blob1 not entirely self consistent

backup

blazar flares

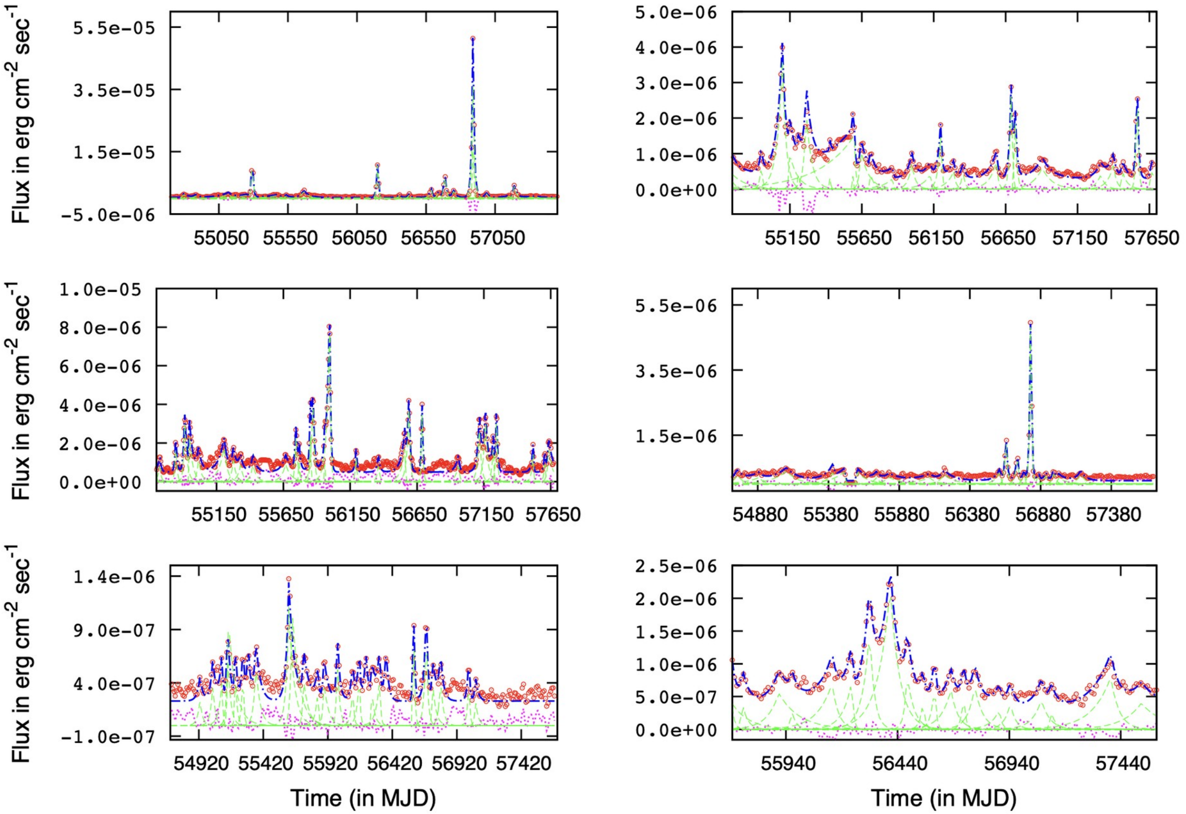

Figure 1. *Top left* – 3C 279; *top right* – 3C 273; *middle left* – 1510-089; *middle right* – Mrk 501; *bottom left* – PKS 2155-304; *bottom right* – PKS 1424-41. The red open circles denote the *Fermi*-LAT light curves of the above blazars at the energy range 0.1–300 GeV, which are smoothed with a Gaussian function of width 10 days; green long-dashed lines represent the individual decomposed flares (see the text), the blue dot–dashed line is the best fit to the model function given in Section 3.1, which is the sum of the individual flares, while the magenta dotted line is the residue after the fit.

Roy et al. 2019

For example *Roy et al. 2019* :

Study of long-term (~weeks–months) and short-term (~hour–day) GeV flares in a sample of 10 blazars from the Fermi-LAT and the Yale/SMARTS monitoring programme.

→ symmetric flares : dominated by the crossing time-scale of a disturbance ?

→ asymmetric flares : signature of gradual particle acceleration and cooling ?

injection & adiabatic expansion

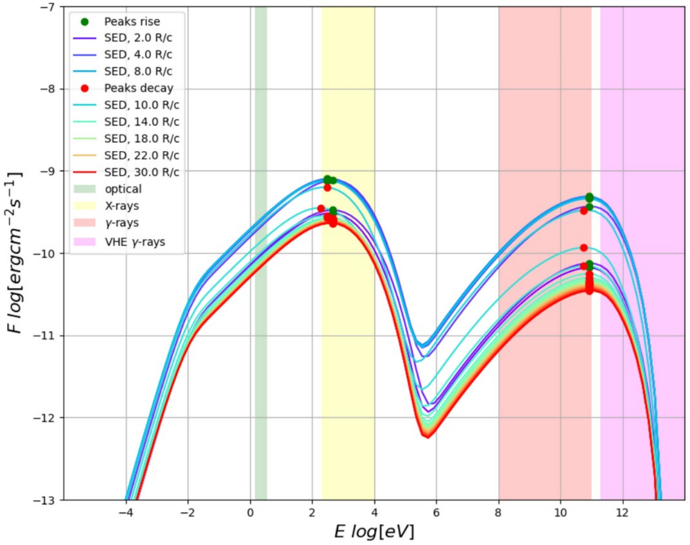

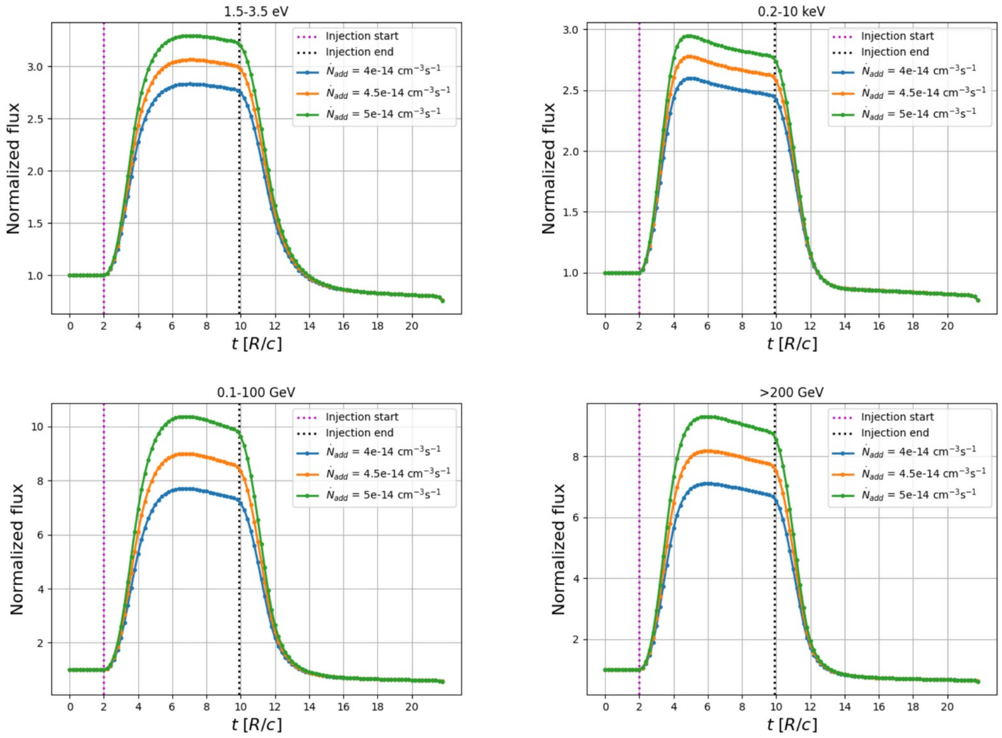

Fermi-II acceleration

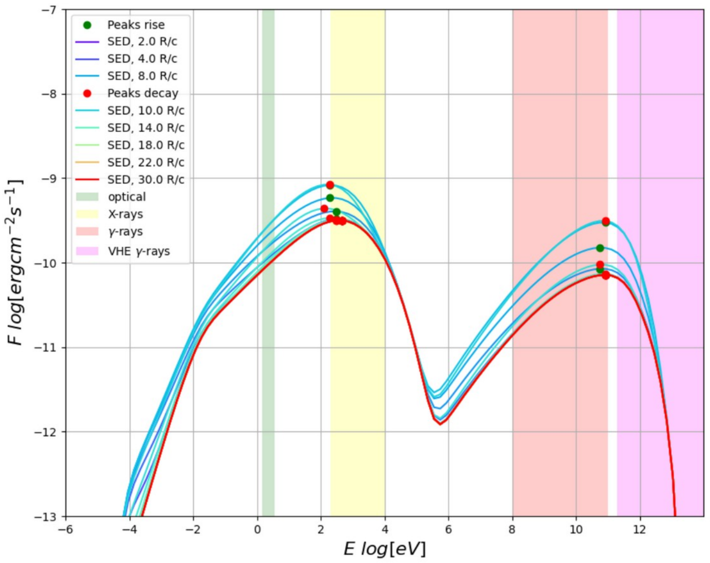

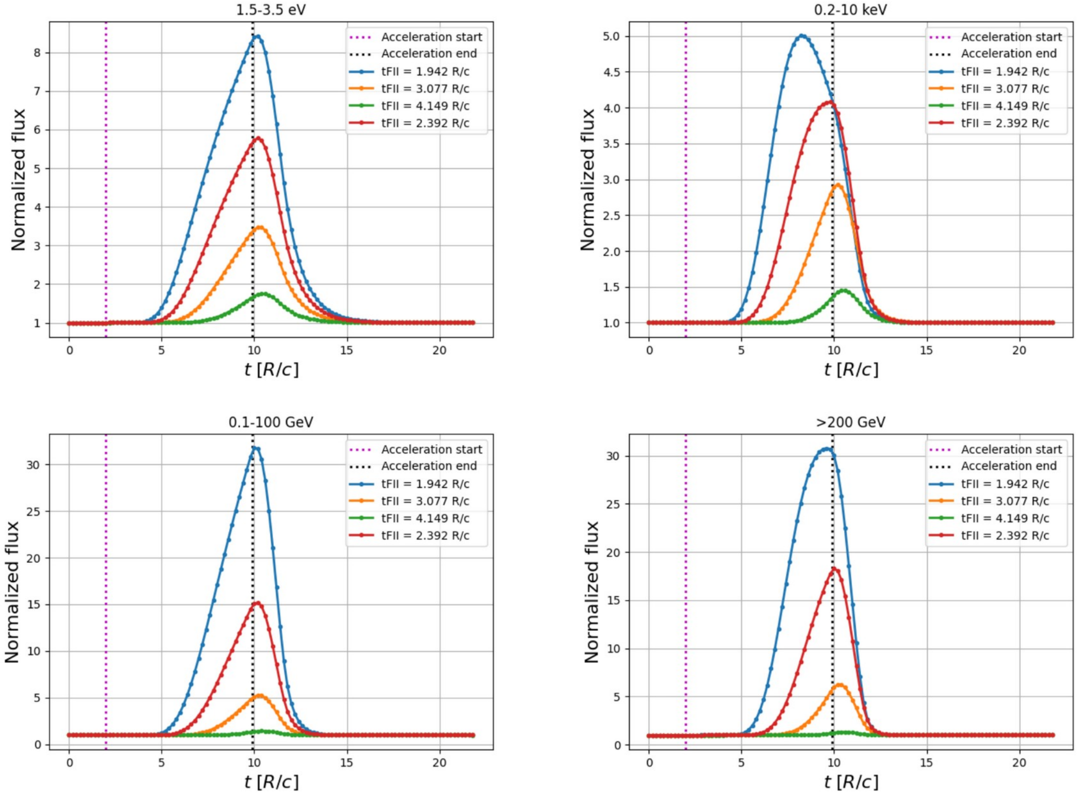

Fermi-I re-acceleration

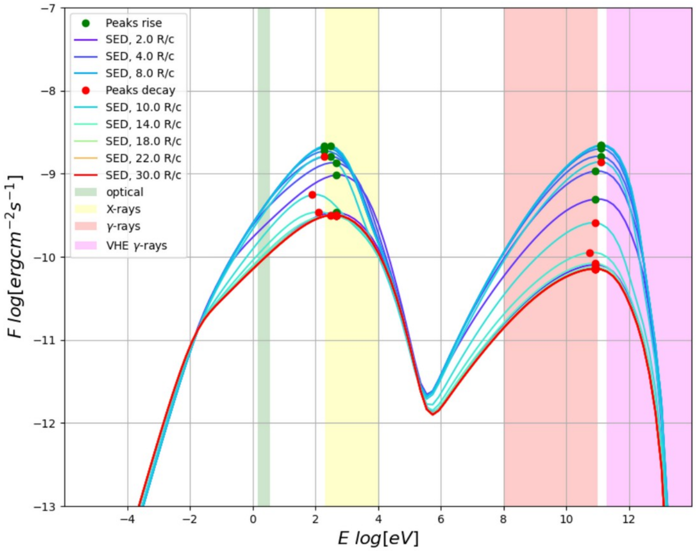

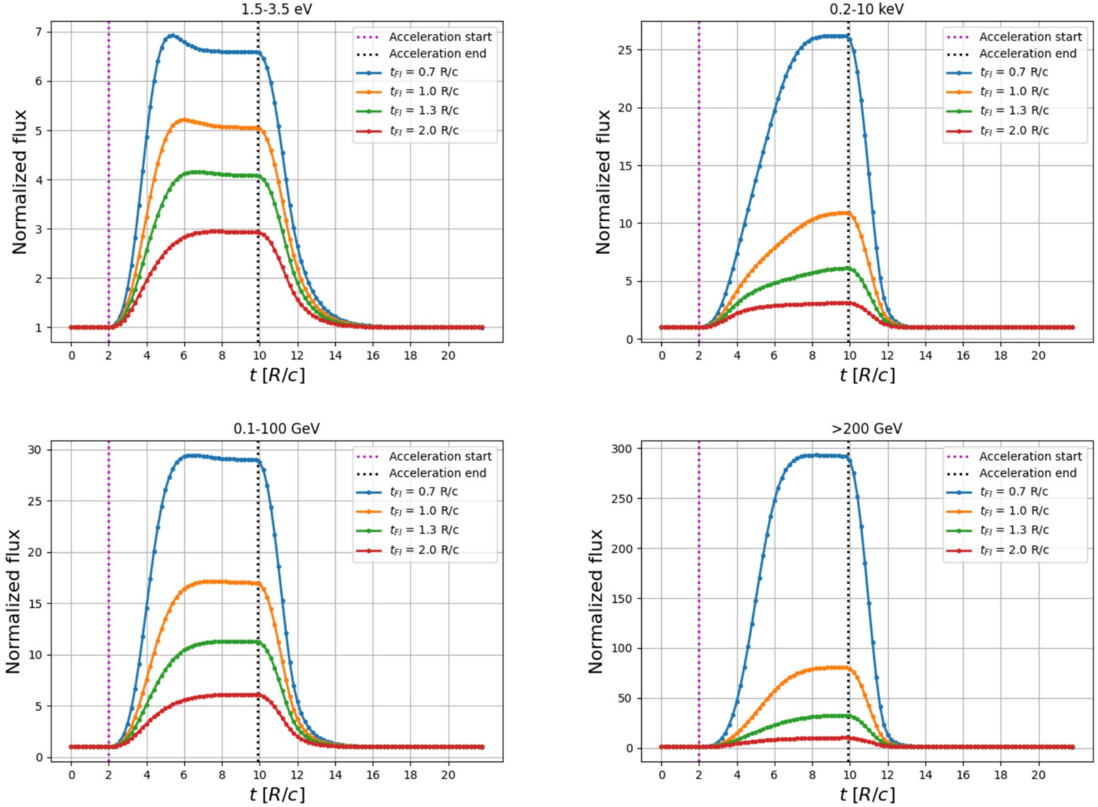

model parameters

	Blob characteristics	Injection spectrum
Blob 1	**Type** : stationary **Magnetic field** $= 2.5\ G$ $R_{b-BH} = 0.5 \times 10^{17}\ cm$ $R_b = 2.1 \times 10^{16}\ cm$	**Type** : PL $\mathbf{N} = 3.0 \times 10^{-4} cm^{-3} s^{-1}$ $\gamma_{pivot} = 215$ $\alpha_{inj} = -3.5$ $\gamma_{min} = 675$ $\gamma_{max} = 10^7$
Blob 2	**Type** = accelerating **Magnetic field** $= [0.01, 0.0086]\ G$ $R_{b-BH} = [0.1, 50] \times 10^{17}\ cm$ $R_b = [2.4, 2.8] \times 10^{16}\ cm$	**Type** = PL $\mathbf{N} = 2.5 \times 10^{-4} cm^{-3} s^{-1}$ $\gamma_{pivot} = 200$ $\alpha_{inj} = -3.5$ $\gamma_{min} = 1300$ $\gamma_{max} = 10^7$

Redshift	$z = 0.536$
Initial Doppler factor	$\delta_i = 18.8$
Final Doppler factor	$\delta_f = 30$
Jet angle	$\theta_j = 1.91°$
Black hole mass	$M_{BH} = 1.0 \times 10^{42}$ g $= 0.5 \times 10^9\ M_\odot$
Disk luminosity	$L_d = 1.0 \times 10^{46}$ erg/s
BLR fraction	$f_{BLR} = 0.1$
BLR power law index	$\beta_{BLR} = 4$
DT fraction	$f_{DT} = 0.1$
DT temperature	$T_{DT} = 1500$ K

particle acceleration in jets

Possibly there is no single mechanism at play, but several mechanisms contribute in different regions of the jet.

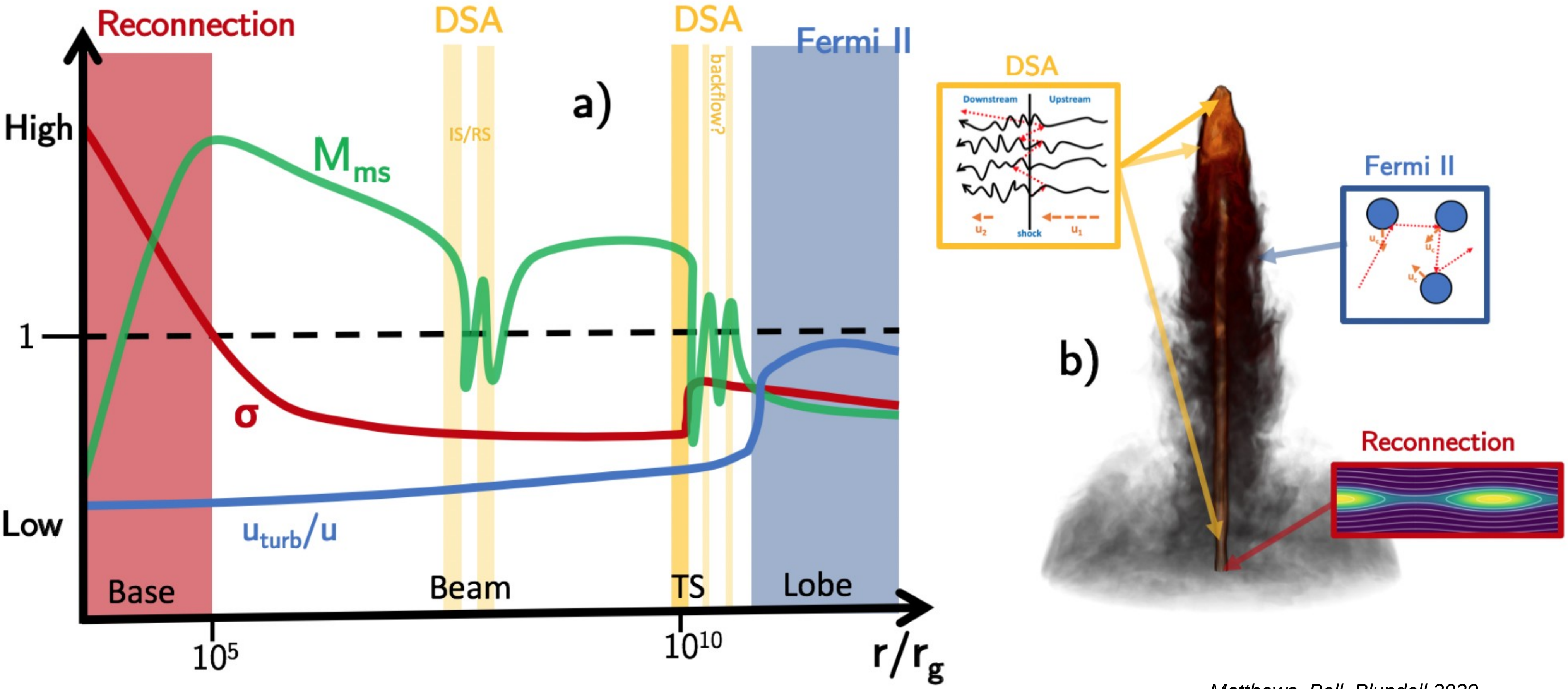

Matthews, Bell, Blundell 2020

an example : modelling a flare from Mrk 421

In this model, the continuous low-state emission from Mrk 421 is connected with a flare in Feb. 2010 :

- low state is modelled with a continuous injection (+ cooling, escape) of electrons accelerated on a (bow) shock into the emitting blob

- the hard spectrum during the flare requires additional Fermi II acceleration from a turbulent emission region surrounding the blob as it passes through an inhomogeneous region inside the jet.

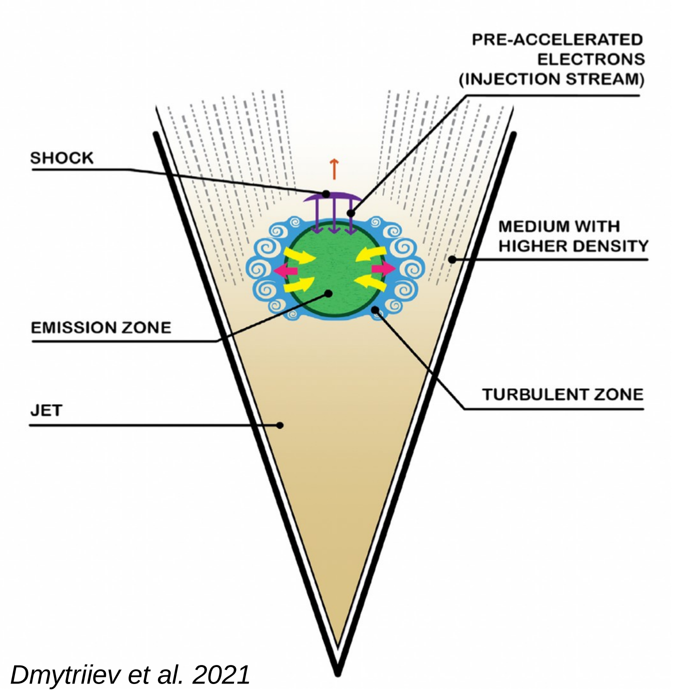

A. Dmytriiev et al. 2021

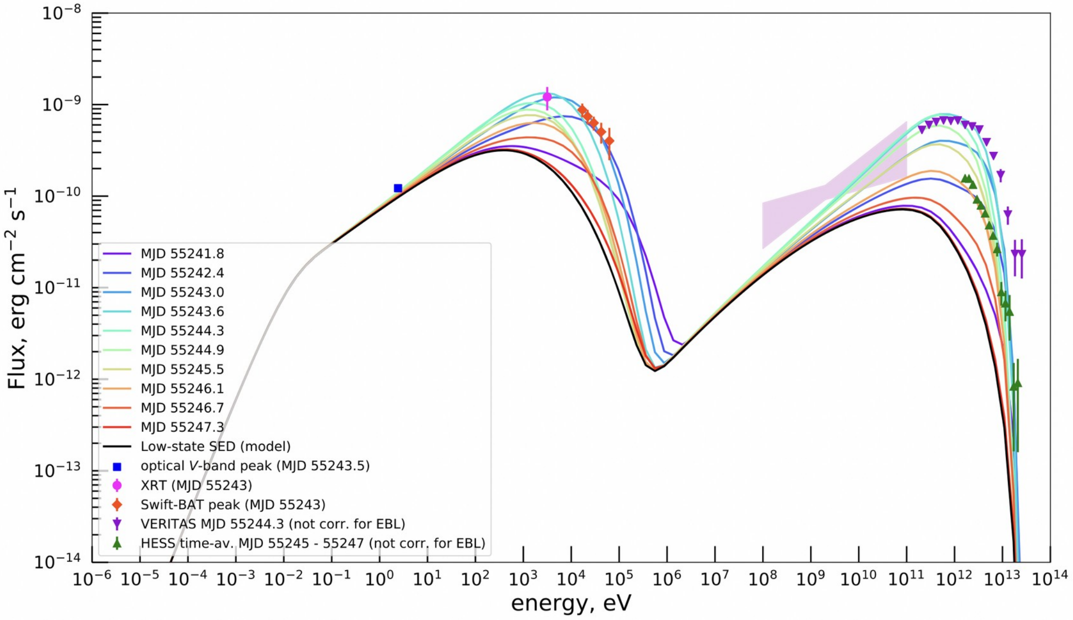

Broad-band emission from Mrk 421 during low state and flare + model curves. (*A. Dmytriiev et al. 2021)*

an orphan flare from 3C 279 in 2013 ?

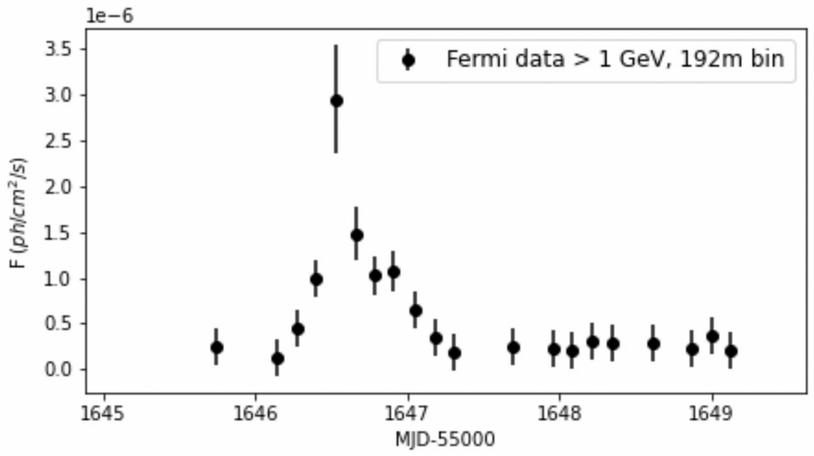

Le Bihan 2024;
with data from Hayashida et al. 2015

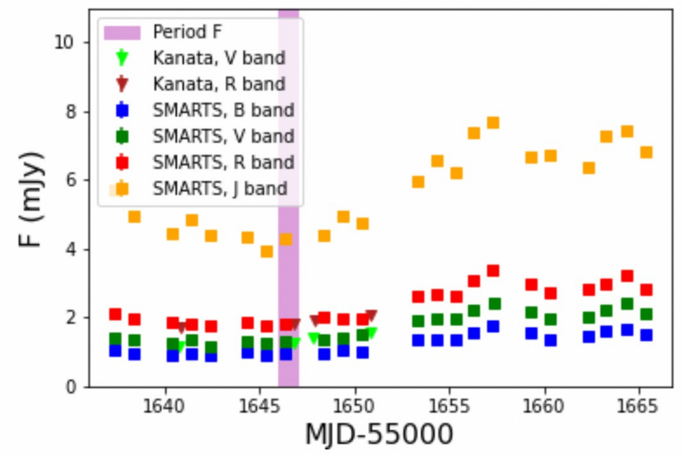

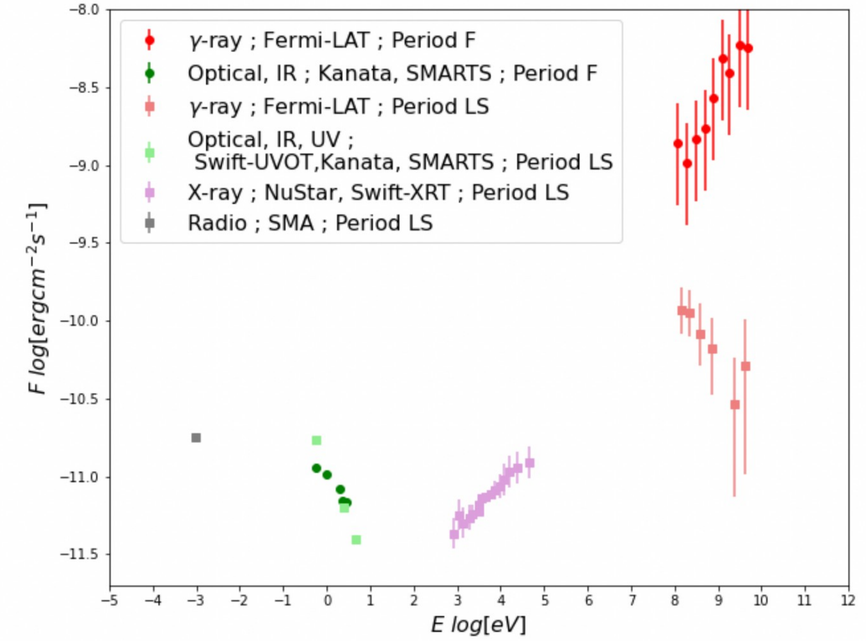

- significant Fermi flare from this FSRQ on 20.12.2013
- no significant variability in simultaneous optical data
- no simultaneous X-ray data

particle acceleration in jets

Several acceleration processes are being discussed to explain the non-thermal particle distribution in blazar jets.

1. Diffusive shock acceleration & Shock drift acceleration (“Fermi I”)

- acceleration on standing or moving shocks (that might be identified with radio knots)

- power-law distribution of particle energies with an index of ~ 2.2 for mildly relativistic shocks

- requires low magnetization to be efficient: $\sigma = \frac{u_B}{u_{particles}} \prec 10^{-2}$

2. Stochastic acceleration by turbulence (“Fermi II”)

- acceleration on turbulences that can be caused by Kelvin-Helmholtz instabilities at interfaces between different jet layers or knots, or by magnetic instabilities.

- power-law / logparabola distribution of particle energies with hard spectra

- in general, less efficient than Fermi I

particle acceleration in jets

3. Shear acceleration

- acceleration through scattering of shearing flows at different velocities (interface jet / ambient medium , interface between different jet layers…) through Fermi-like process.

- The distribution of accelerated particles tends to a power law with index depending on the properties of the underlying turbulence.

4. Magnetic reconnection

- acceleration through energy realease in regions of reorganisation of magnetic field lines

- can lead to power-law distribution with very hard index ~1.5 – 1 for high magnetization

- requires high jet magnetization to be efficient $\sigma \gg 1$

5. Pulsar-like acceleration in the BH magnetosphere

the VLBI – high-energy connection

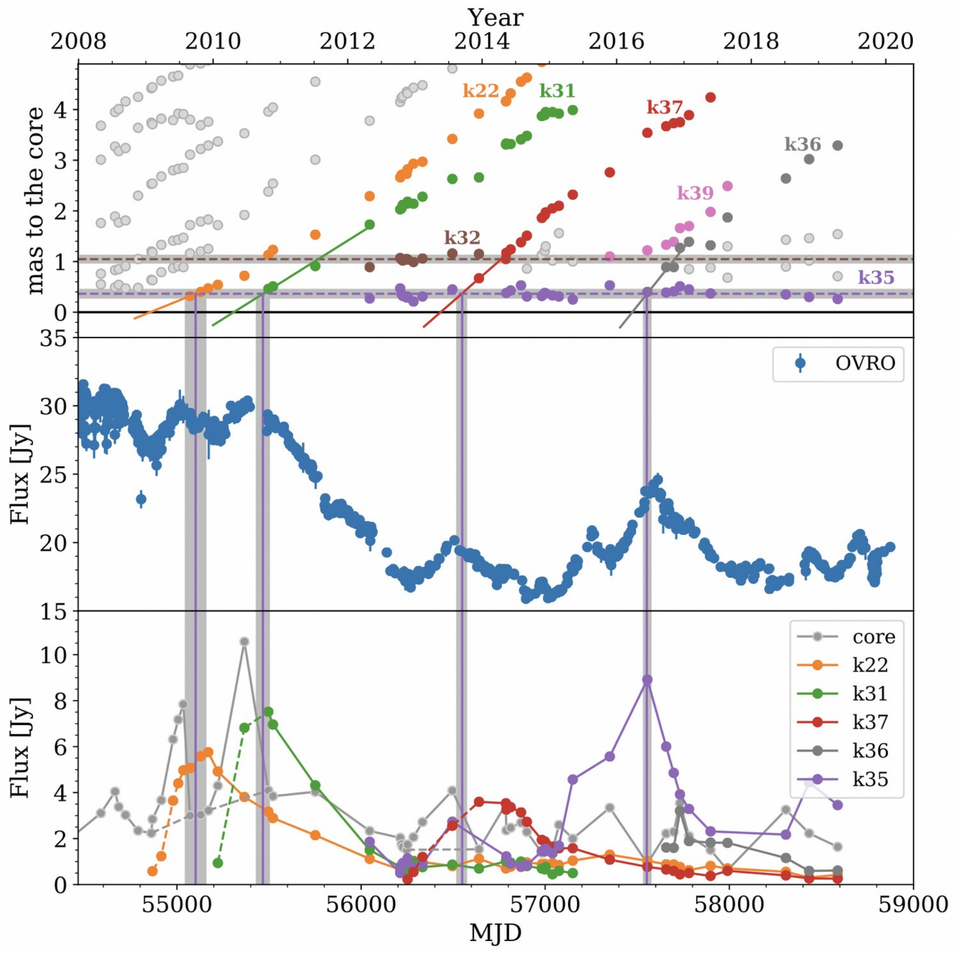

blazar 3C 273 observed at 15.3 GHz

upper panel : identification of moving and standing radio knots with the Mojave VLBI survey

middle panel : light curve of the overall radio flux from the jet

bottom panel : light curves of radio fluxes from individual knots

→ The crossing of moving knots through the position of standing knots coincides with flux increases in the moving knots. These are also visible in the overall emission, if they are isolated events.

→ Indication of **shock-shock interactions** inside the jet.

Fichet de Clairfontaine et al. (2020)

beyond the one-zone model

shock-shock interactions in an MHD jet

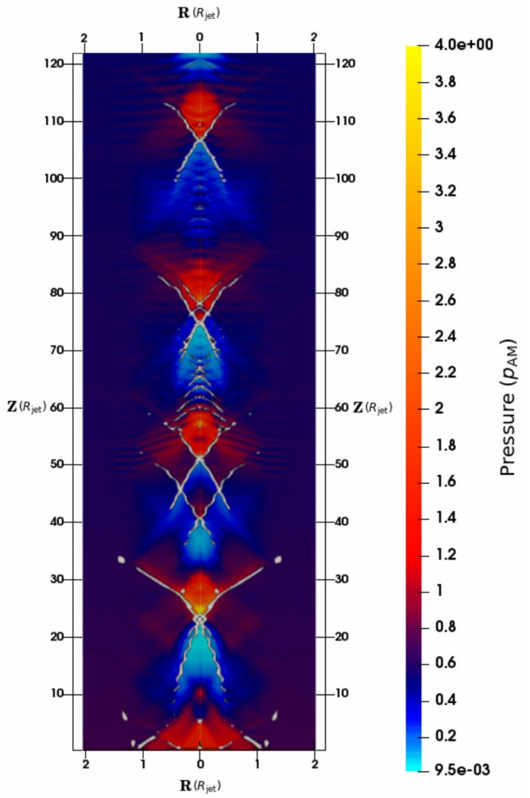

rarefaction (light blue) and compression (red) regions and associated standing shocks (white)
G. Fichet de Clairfontaine et al. 2021

In this example, an overpressured jet propagates in the ambient medium.

→ formation of a series of recollimation shocks (left)

A perturbation (= zone with elevated Lorentz factor or density) is injected at the base of the jet. A bow shock forms in front of the pertubation as it propagates through the jet.

→ shock-shock interactions lead to enhanced emission (i.e. flares), here observed in the radio band

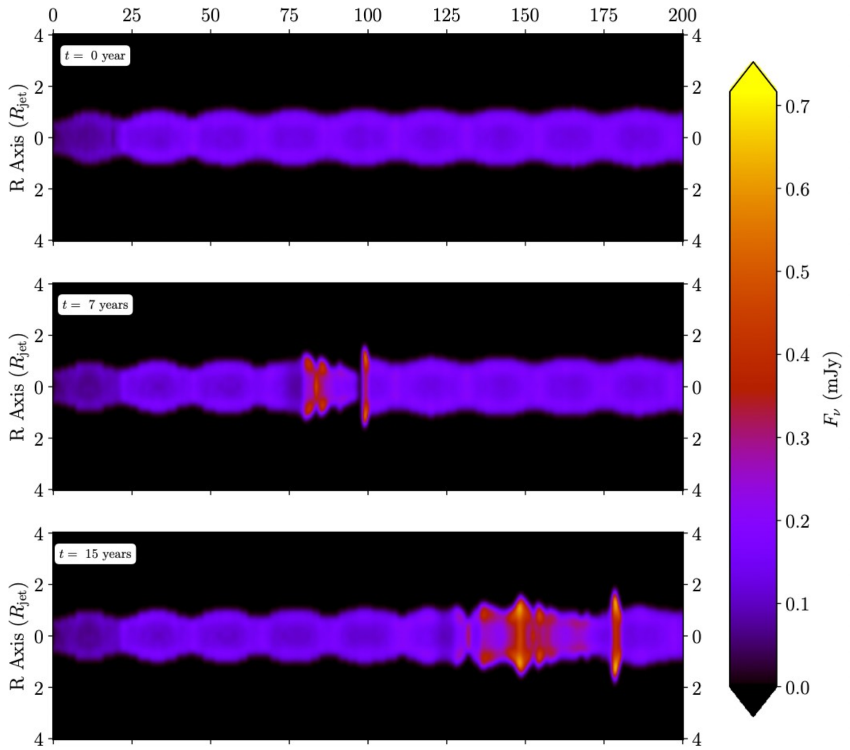

radio (synchrotron) emission from a perturbation crossing standing shocks
G. Fichet de Clairfontaine et al. 2022